Computer Assisted Mechanics and Engineering Sciences, 8: 17–44, 2001.

Computational problems of FE-analysis of elastic-plastic surface structures

J. Bielski
Institute of Mechanics and Machine Design, Cracow University of Technology
ul. Warszawska 24, 31-155 Cracow, Poland

M. Radwańska
Institute of Computer Methods in Civil Engineering, Cracow University of Technology
ul. Warszawska 24, 31-155 Cracow, Poland

(Received July 15, 1999)

The paper contains a review of problems connected with numerical analysis of elastic-plastic surface structures. Given is detailed information about finite elements as well as about the algorithm of physically non-linear analysis using the incremental-iterative Newton–Raphson method with the consistent modular matrix. The main goal of the paper is to compare numerical results obtained with elements based on either the volume or area approach to the formulation of physical relations. The presented examples are obtained with the use of computer code *MANKA*. They illustrate some numerical problems induced by elastic-plastic deformation of chosen types of plates.

Keywords: material non-linearity, FEM, volume/area approach

NOTATION

B, S, E, P	– the level of analysis: structure (body), cross-section, element, point, respectively,
GPLY	– Gauss point with co-ordinates (ξ, η, ζ) in a layer $\zeta = \text{const}$,
LBPT	– Lobatto point with co-ordinates (ξ, η, ζ) on a thickness director,
GPMS	– Gauss point with co-ordinates $(\xi, \eta, 0)$ on the midsurface,
$IE = 1, \ldots, NE$	– numbers of finite elements,
$ILY = 1, \ldots, NLY$	– numbers of layers,
$ILB = 1, \ldots, NLB$	– numbers of Lobatto integration points,
$IGLY = 1, \ldots, NG$	– numbers of Gauss integration points over a layer surface,
$IGMS = 1, \ldots, NG$	– numbers of Gauss integration points over the midsurface,
$[m]$	– number of an increment of a control parameter (time-step),
(i)	– number of a global equilibrium iteration,
(k)	– number of an iteration for integration of constitutive relations,

ξ, η – isoparametric co-ordinates in a parent finite element,

z, ζ – co-ordinate along the thickness direction (dimensional and dimensionless),

$\mathbf{x}_0$, $\hat{\mathbf{x}}$ – position vector of a point on a reference surface (midsurface), orientation of a vector initially normal to the reference surface,

$\mathbf{x}$ – position vector of a point with co-ordinates (ξ, η, ζ),

$\mathbf{d}_0$, $\hat{\mathbf{d}}$ – displacement vector of a midsurface point; relative displacement vector of point $\hat{x}$,

$\mathbf{d}$ – displacement vector of a point with co-ordinates (ξ, η, ζ) — *GPLY* or *LBPT* point,

$\mathbf{J}_0$, $\mathbf{J}$ – Jacobian transformation matrices from local to global co-ordinate system for a midsurface point or a distant surface point, respectively,

$\boldsymbol{\sigma}$, $\Delta\boldsymbol{\sigma}$ – stress and stress increment vectors at *ILY* layer or at *ILB* point,

$\boldsymbol{\varepsilon}$, $\Delta\boldsymbol{\varepsilon}$ – strain and strain increment vectors at *ILY* layer or at *ILB* point,

$\Delta\boldsymbol{\varepsilon}^{pl}$ – plastic strain increment vector,

$\mathbf{S}$, $\bar{\mathbf{S}}$ – dimensional and dimensionless resultant stress vector at *IGMS* point,

$\mathbf{e}$, $\bar{\mathbf{e}}$ – dimensional and dimensionless generalised strain vector at *IGMS* point,

$\mathbf{E}$ – elasticity matrix,

$\mathbf{D}$ – constitutive resultant matrix,

$\mathbf{P}$ – plasticity matrix,

p, ϵ_p, κ_p – hardening parameter, the Odquist parameter, equivalent plastic curvature,

$\Delta\lambda$ – plastic multiplier,

$\mathbf{q}$, $\Delta\mathbf{q}$ – nodal displacement vector and its increment on level E,

$\mathbf{Q}$, $\Delta\mathbf{Q}$ – nodal displacement vector and its increment on level B in $\Re^N$ space,

$\tau = \Lambda$, $\tau = Q_j$ – control parameter (load or displacement control),

Λ – load parameter (multiplier),

p^* – reference load,

$\mathbf{F}^*_{\text{ext}}$ – reference external nodal load vector,

$\mathbf{F}_{\text{int}}(\mathbf{Q})$ – vector of internal forces dependent on current displacements,

$\mathbf{R}(\mathbf{Q}, \Lambda) = \mathbf{F}_{\text{int}}(\mathbf{Q}) - \Lambda\mathbf{F}^*_{\text{ext}}$ – residual forces vector,

$\mathbf{K}_T$ – tangent stiffness matrix,

$\mathbf{t}$ – control vector.

$\mathbf{y}$ vector is a one-column matrix, $\mathbf{y} = \begin{bmatrix} y_1 \\ \vdots \\ y_N \end{bmatrix} = \{ y_1 \ \cdots \ y_N \}$.

1. Introduction

The aim of the paper is to present all steps of a numerical analysis of elastic-plastic surface structures. Hence, we describe the strategy of the incremental-iterative solution on the level of discretised

structure, which is coherent with integration of the incremental physical relations on the point level where the consistent tangent matrix is employed. Three types of finite elements are used within the displacement finite element formulation. Two approaches are compared in the paper — volume-based and area-based — each referred to a different definition of stress vector or resultant stress vector. The volume approach means that the constitutive equations are formulated and solved at all discretization points along the thickness and then stresses are integrated to obtain the generalised stresses on the middle surface. The area approach means that the constitutive relations are formulated and solved in terms of the resultant stresses directly and no along-the-thickness integration is performed. The degenerated-continuum-theory or the plate theory is applied for finite element formulation. For the latter case the Reissner–Mindlin formulation is applied to moderately thin surface structures with transverse shear included. The presented description of finite elements gives a complete set of definitions and relations which are necessary for computational implementation (i.e. approximation of geometry, displacement field, strains, stresses). The displacements, rotations and strains are assumed to be small and material non-linearity is only analysed. The plastic flow rule associated with the Huber–von Mises plasticity condition is employed. The plastic hardening is included in models based on the volume approach whereas for those based on the area approach perfect plasticity is assumed. The employed formulae and flow charts of algorithms are collected. The collections are intended to make the computer implementation straightforward. The described elements are implemented in the *MANKA* code. Numerical examples deal with either the bending state or coupling of bending and membrane states.

The authors realise that there are many other problems to be encountered when the class of problems is broadened beyond linear elasticity. This paper, addressed mainly for 'beginners', puts a stress on some problems connected with non-linear, elastic-plastic physical laws and known algorithms of solving them. For more details and discussion of geometrical nonlinearities (large displacements, large strains), relaxing the Reissner–Mindlin assumption, thermal effects, numerical problems of different types of locking and other related problems, the reader is referred to literature — for example [6, 13, 14, 30] and lists of references therein. However, one should realise that there are a lot of books, papers and conference proceedings dealing with these subjects, not invoked here.

2. Theoretical background

2.1. Strategy of numerical analysis of elastic-plastic surface structures

The numerical analysis of non-linear elastic-plastic surface structures combines computational techniques with surface structures mechanics, theory of plasticity and finite element method algorithms. The authors have been involved for some years in numerical analysis of such structures [1–3, 10, 17, 28].

Aiming at lucidity of the presented computational algorithm the different levels of analysis are named after the monograph [31]: i) point P, ii) cross-section S, iii) finite element E, iv) assembled system of finite elements also called body B. Using the incremental-iterative algorithm for the non-linear analysis one deals with repetitive transitions between the levels: $\mathsf{B} \to \mathsf{E} \to \mathsf{S} \to \mathsf{P} \to \mathsf{S} \to \mathsf{E} \to \mathsf{B} \to \ldots$

Tracing the deformation of a structure is based on the formulation and solving of the initial-boundary value problem. Implementation of the FE method demands both spatial and time discretization. For the incremental formulation of the materially non-linear problem the sequence of following states of a structure is determined for the increasing value of a time-like parameter ${}^{[m]}\tau$. For a sequence of increments $\Delta\tau$ the Newton method is applied on the structure level B, as well as on the point level P while integrating the elastic-plastic constitutive relations. Various formulations of finite elements are possible for the analysis of surface structures. Even for the elastic range the analysis of plates and shells (thin, moderately thick, thick) is based on either two- or three-dimensional treatment. Beyond the elastic range, in general, one deals with the three-dimensional discretization, despite the assumption that the thickness is considerably smaller than the midsurface dimensions.

That is the result of the fact that the along-thickness stress distribution is not known in advance. Moreover, it is usually necessary to determine the spread of the plastic zones with respect to all three dimensions of a structure.

The transition between two following states of a structure is described by the incremental relations coming up from the virtual work principle [26, 27, 28]

$$\sum_{IE=1}^{NE} \int_{\Omega_e} (\delta\Delta\boldsymbol{\varepsilon})^T (\boldsymbol{\sigma} + \Delta\boldsymbol{\sigma})\, \mathrm{d}\Omega = \sum_{IE=1}^{NE} \int_{\Omega_e} (\delta\Delta\mathbf{d})^T (\mathbf{p} + \Delta\mathbf{p})\, \mathrm{d}\Omega. \tag{1}$$

When using the displacement-based finite element method it is assumed that incremental kinematic and physical relations are satisfied, $\Delta\boldsymbol{\sigma} = \Delta\boldsymbol{\sigma}(\Delta\boldsymbol{\varepsilon}(\Delta\mathbf{d}))$, whereas finite element approximation relates to the generalised displacement field $\mathbf{d} = \mathbf{d}(\mathbf{q})$. Combining translational and rotational nodal degrees of freedom the vectors $\mathbf{q}$ and $\mathbf{Q}$ together with their increments are built on the element level E and the structure level B, respectively. The solution of so-called extended set of incremental equations is sought for in the displacement–load subspace of $\Re^{N+1}$ [27]

$$\tilde{\mathbf{K}}_T \, \Delta\Delta\tilde{\mathbf{Q}} = \tilde{\mathbf{R}}, \tag{2}$$

where the following notation is used:

$\Delta\Delta\tilde{\mathbf{Q}} = \{\Delta\Delta\mathbf{Q},\, \Delta\Lambda\}$, $\quad \tilde{\mathbf{R}} = \{\mathbf{R},\, \Delta\tau\}$,

$\Delta\Delta\mathbf{Q}$ – subincrement of displacements,

$\Delta\tau$ – increment of a time-like control parameter,

$\Delta\Lambda$ – increment of a load parameter.

The extended set consists of equations for finite elements

$$\mathbf{K}_T \cdot \Delta\Delta\mathbf{Q} - \Delta\Lambda\, \mathbf{F}^*_{\mathrm{ext}} = \mathbf{R} \tag{3}$$

completed with the constraint equation

$$\mathbf{t}^T \Delta\Delta\mathbf{Q} + t_{N+1}\, \Delta\Lambda = \Delta\tau. \tag{4}$$

The structure of the extended set of incremental equations is illustrated in Fig. 1.

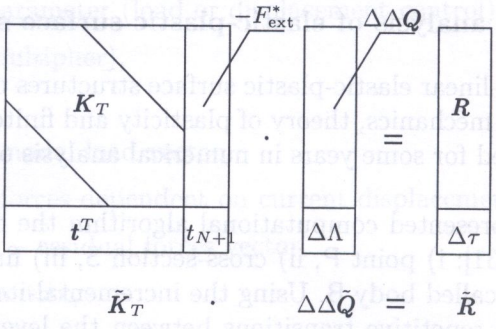

Fig. 1. Structure of extended set of incremental equations

The continuation process is controlled by means of the control vector $\tilde{\mathbf{t}} = \{\mathbf{t},\, t_{N+1}\}$. Usually, either a specified nodal displacement or the load parameter is chosen.

For the discrete continuation method we use, the iteration procedure induces intermediate configurations, which in turn implies introduction of subincrements for the generalised displacements (Fig. 2). Hence, on level B one starts from known displacements ${}^{[m]}\mathbf{Q}$ for a given $[m]$-th equilibrium state in order to obtain a new displacement vector ${}^{[m+1]}\mathbf{Q}$ in an iterative way

$$\begin{aligned} {}^{[m+1]}\mathbf{Q} &= {}^{[m]}\mathbf{Q} + \Delta\mathbf{Q} = {}^{[m]}\mathbf{Q} + \Delta\Delta\mathbf{Q}^{(1)} + \Delta\Delta\mathbf{Q}^{(2)} + \cdots + \Delta\Delta\mathbf{Q}^{(i-1)} + \Delta\Delta\mathbf{Q}^{(i)} \\ &= {}^{[m+1]}\mathbf{Q}^{(i-1)} + \Delta\Delta\mathbf{Q}^{(i)}. \end{aligned} \tag{5}$$

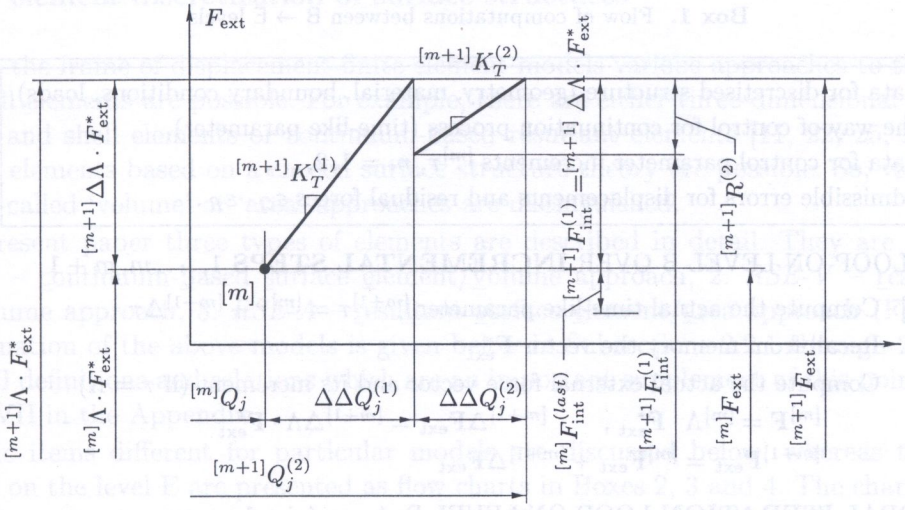

Fig. 2. Notation for calculations with Newton–Raphson method

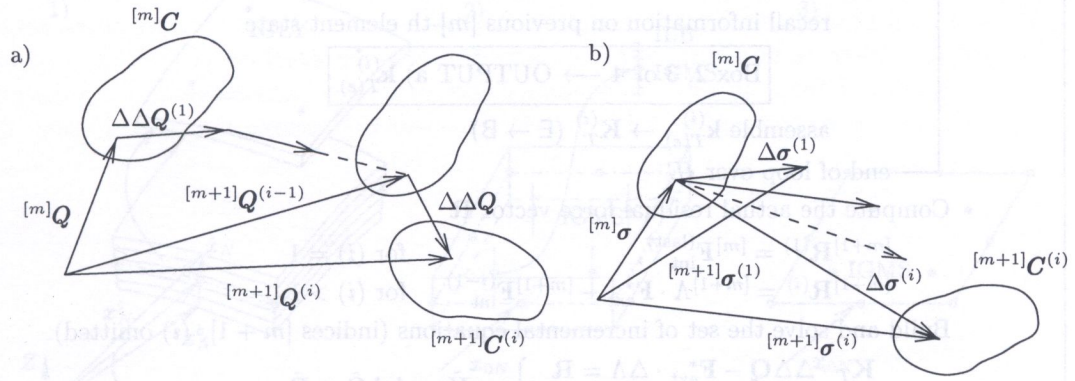

Fig. 3. Sketch of iteration process; a) on structure level B, b) on point level P

Two different increment schemes are illustrated in Fig. 3a,b. The first relates to level B (and simultaneously, to the displacement space) whereas the second — to level P (stress space). The latter scheme is employed to update stresses basing on the obtained displacement field for the $[m]$-th equilibrium state. The scheme is constructed in order to ensure the path-independence of the calculated deformations during the iteration process. The incremental equations on level B are coupled with the incremental physical and kinematic relations $\Delta\boldsymbol{\sigma} = \Delta\boldsymbol{\sigma}(\Delta\boldsymbol{\varepsilon}(\Delta\mathbf{d}))$ formulated on level P. The iterative scheme for updating stresses is

$$^{[m+1]}\boldsymbol{\sigma}^{(i)} = {}^{[m]}\boldsymbol{\sigma} + \Delta\boldsymbol{\sigma}^{(i)}. \tag{6}$$

It is emphasised that all level P variables are only updated after the iteration process for level B is completed.

The general incremental-iterative algorithm is shown by the flow chart in Box 1. It presents the sequence of calculations performed between levels B and E for a sequence of incremental steps $[1, 2, \ldots, m, (m+1)]$ and iterative steps $(1, 2, \ldots, i, (i+1))$. The matrix $\mathbf{K}_T$ and vector $\mathbf{F}_{\text{int}}$ used in the Box 1 are calculated according to a finite element model applied.

Box 1. Flow of computations between B → E levels

INPUT: data for discretised structure (geometry, material, boundary conditions, loads),
the way of control for continuation process (time-like parameter),
data for control parameter increments ${}^{[m]}\tau$, $m = 1, 2, \ldots$,
admissible errors for displacements and residual forces ε_Q , ε_R .

→ GLOBAL LOOP ON LEVEL B OVER **INCREMENTAL STEPS** $1, \ldots, m, m+1$

For $[m+1]$: Compute the actual time-like parameter ${}^{[m+1]}\tau = {}^{[m]}\tau + {}^{[m+1]}\Delta\tau$

Recall from memory the vector $\mathbf{F}^*_{\text{ext}}$

Compute the actual external force vector and its increment (if $\tau = \Lambda$)

$${}^{[m]}\mathbf{F} = {}^{[m]}\Lambda \cdot \mathbf{F}^*_{\text{ext}}\,, \qquad {}^{[m+1]}\Delta\mathbf{F}_{\text{ext}} = {}^{[m+1]}\Delta\Lambda \cdot \mathbf{F}^*_{\text{ext}}$$

$${}^{[m+1]}\mathbf{F}_{\text{ext}} = {}^{[m]}\mathbf{F}_{\text{ext}} + {}^{[m+1]}\Delta\mathbf{F}_{\text{ext}}$$

→ GLOBAL **ITERATION** LOOP ON LEVEL B, $1, \ldots, i, i+1, \ldots$

Recall displacement vector ${}^{[m]}\mathbf{Q}^{(\text{last})}$ for $i = 1$ or ${}^{[m+1]}\mathbf{Q}^{(i-1)}$ for $i > 1$

Compute the actual tangent stiffness matrix ${}^{[m+1]}\mathbf{K}_T^{(i)}$

→ loop over finite elements $IE = 1, \ldots, NE$

recall information on previous $[m]$-th element state

Box 2, 3 or 4 ⟶ OUTPUT a) $\mathbf{k}^{(i)}_{T(e)}$

assemble $\mathbf{k}^{(i)}_{T(e)} \to \mathbf{K}^{(i)}_T$ (E → B)

— end of loop over IE

Compute the actual residual force vector $\mathbf{R}$

$${}^{[m+1]}\mathbf{R}^{(1)} = {}^{[m]}\mathbf{F}^{(\text{last})}_{\text{int}}, \qquad \text{for } (i) = 1$$

$${}^{[m+1]}\mathbf{R}^{(i)} = {}^{[m+1]}\Lambda \cdot \mathbf{F}^*_{\text{ext}} - {}^{[m+1]}\mathbf{F}^{(i-1)}_{\text{int}}, \quad \text{for } (i) > 1$$

Build and solve the set of incremental equations (indices $[m+1]$, (i) omitted)

$$\left.\begin{aligned} \mathbf{K}_T \cdot \Delta\Delta\mathbf{Q} - \mathbf{F}^*_{\text{ext}} \cdot \Delta\Lambda &= \mathbf{R} \\ \mathbf{t}^T \cdot \Delta\Delta\mathbf{Q} + t_{N+1} \cdot \Delta\Lambda &= \Delta\tau \end{aligned}\right\} \to \tilde{\mathbf{K}}_T \cdot \Delta\Delta\tilde{\mathbf{Q}} = \tilde{\mathbf{R}}$$

Calculate the subincrement of the displacement vector ${}^{[m+1]}\Delta\Delta\mathbf{Q}^{(i)}$

Add subincrement to the total displacement vector

$${}^{[m+1]}\mathbf{Q}^{(i)} = {}^{[m+1]}\mathbf{Q}^{(i-1)} + {}^{[m+1]}\Delta\Delta\mathbf{Q}^{(i)}$$

Compute the actual internal force vector ${}^{[m+1]}\mathbf{F}^{(i+1)}_{\text{int}}$

→ loop over finite elements $IE = 1, \ldots, NE$

use information on $[m+1]$-th element state

Box 2, 3 or 4 ⟶ OUTPUT b) $\mathbf{f}^{(i)}_{(e)}$

assembling $\mathbf{f}^{(i+1)}_{(e)} \to {}^{[m+1]}\mathbf{F}^{(i+1)}$ (E → B)

— end of loop over IE

Check convergence

$\left\|{}^{[m+1]}\Delta\Delta\mathbf{Q}^{(i)}\right\| < \varepsilon_Q$ and $\|R\| =$	$\left\|{}^{[m+1]}\mathbf{F}_{\text{ext}} - {}^{[m+1]}\mathbf{F}^{(i+1)}_{\text{int}}\right\| < \varepsilon_R$
0	**1**
↓	↓
next iteration $(i) \to (i+1)$	store information on current $[m+1]$-th structure state go to next increment

2.2. Finite element discretization of surface structures

Even within the frame of displacement finite element models various approaches to the foundations of plate/shell elements are possible. For example, there are either three-dimensional or continuum-based plate and shell elements or continuum-based resultant elements [11, 22, 25, 29]. Also, two-dimensional elements based on a chosen surface structure theory are possible. So, various elements based on so-called 'volume' or 'area' approaches are distinguished.

In the present paper three types of elements are described in detail. They are referred to as: 1. *CBSE-V* – continuum-based surface element/volume approach, 2. *RSE-V* – resultant surface element/volume approach, 3. *RSE-A* – resultant surface element/area approach (Fig. 4). The detailed explanation of the above models is given below in Subsections 2.2.1 through 2.2.3. For completeness, all definitions and relations which are an important supplement of this point are collected in Boxes I–VII in the Appendix.

The basic items different for particular models are discussed below, whereas the schemes of calculations on the level E are presented as flow charts in Boxes 2, 3 and 4. The charts in boxes are recalled in the main algorithm of numerical analysis. The calculation schemes for element matrix $\mathbf{k}_T^e$ and vector $\mathbf{f}_{\text{int}}^e$ are also given in the boxes.

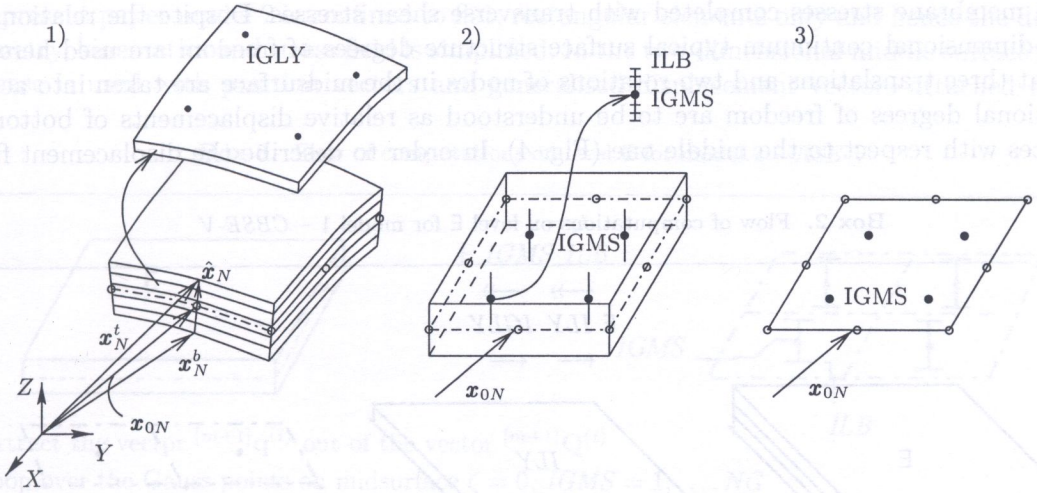

Fig. 4. Analysed FE models: 1) *CBSE-V* 2) *RSE-V* 3) *RSE-A*

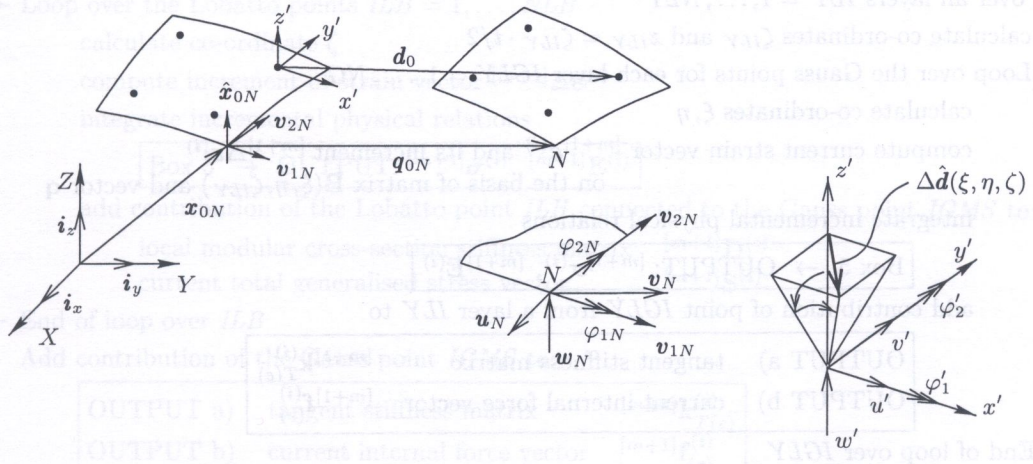

Fig. 5. Description of geometry and kinematics

For all three elements presented in the paper the eight-node base in the middle surface is assumed. Five degrees of freedom are used at each node. Elements of each type employ the base of serendipity shape functions (Box 1). Linear functions of co-ordinate z are employed for the thickness direction for the geometry as well as for displacements and strains. In all types of elements the membrane, bending and transverse shear effects are included.

The mapping from a parent element with (ξ, η, ζ) co-ordinate system onto the current geometry of an element with (x, y, z) co-ordinate system is used, regardless of the element model. For the description of curved elements additional thickness directors $\hat{\mathbf{x}}_{0N}$ are necessary beside the standard position vectors $\mathbf{x}_{0N}$.

The integration over volume or area is performed in various ways and hence the precise notation for discrete points (Gauss or Lobatto) is introduced (see notation and figures).

The merit of integration of the incremental physical relations together with a form of plasticity condition in appropriate stress space (various for different element types) is discussed below and illustrated in Boxes 5, 6.

2.2.1. Model 1

The element *CBSE-V* is based on the volume approach (Fig. 4-1). It is to be seen as a pile of layers, each with membrane stresses completed with transverse shear stresses. Despite the relations with the three-dimensional continuum typical surface structure degrees of freedom are used here. This means that three translations and two rotations of nodes in the midsurface are taken into account. The rotational degrees of freedom are to be understood as relative displacements of bottom and top surfaces with respect to the middle one (Fig. 4). In order to describe the displacement field in

Box 2. Flow of computations on level E for model 1 – *CBSE-V*

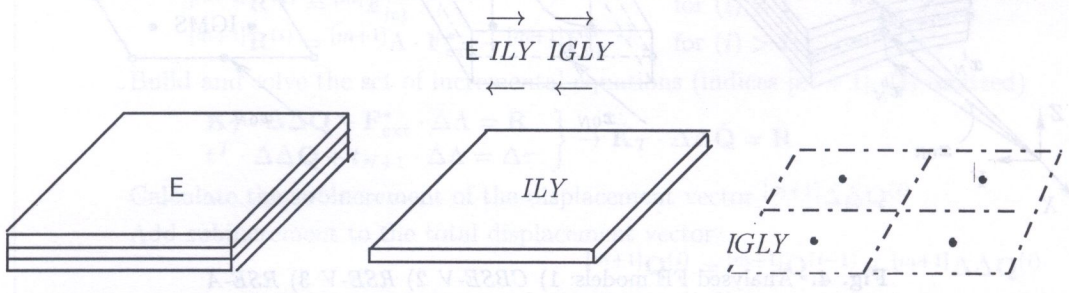

Extract the vector $^{[m+1]}\mathbf{q}^{(i)}$ out of the vector $^{[m+1]}\mathbf{Q}^{(i)}$

→ Loop over all layers $ILY = 1, \ldots, NLY$

calculate co-ordinates ζ_{ILY} and $z_{ILY} = \zeta_{ILY} \cdot t/2$

→ Loop over the Gauss points for each layer $IGLY = 1, \ldots, NG$

calculate co-ordinates ξ, η

compute current strain vector $^{[m+1]}\boldsymbol{\varepsilon}^{(i)}$ and its increment $^{[m+1]}\Delta\boldsymbol{\varepsilon}^{(i)}$ on the basis of matrix $\mathbf{B}(\xi, \eta, \zeta_{ILY})$ and vector $\mathbf{q}$

integrate incremental physical relations

Box 5 → OUTPUT: $^{[m+1]}\boldsymbol{\sigma}^{(i)}$, $^{[m+1]}\mathbf{E}^{(i)}$

add contribution of point *IGLY* from a layer *ILY* to

OUTPUT a)	tangent stiffness matrix	$^{[m+1]}\mathbf{k}^{(i)}_{T(e)}$
OUTPUT b)	current internal force vector	$^{[m+1]}\mathbf{f}^{(i)}_{(e)}$

└ End of loop over *IGLY*

└ End of loop over *ILY*

a particular layer the superposition of two fields is employed. The one is a field $\mathbf{d}_0$ defined on the middle surface ($z = 0$) and the other is $\Delta\hat{\mathbf{d}}$ — relative displacements of two external layers $z = \pm\frac{t}{2}$ (Box III, Fig. 4).

The integration over an element volume is performed numerically. At first, the area integration is performed in each layer, then the summation over all layers is done. Hence, a set of the $NG \times NLY$ Gauss points is regarded as the element representative. At each point of each layer ($GPLY$) we deal with five-element stress and strain spaces (Box IV). Components of the resultant stress vector are calculated be means of summation over the layers at each Gauss integration point of the middle surface ($GPMS$) after the stresses in layers are updated.

The derivatives of displacements with respect to the local co-ordinates (present in kinematic relations, Box V) are calculated at the Gauss points $IGLY$ in a standard way: derivatives of shape functions are computed, reverse Jacobian matrix $\mathbf{J}_0$ is used (calculated on the middle surface for thin shells) and transformation matrices $\mathbf{T}_T$ and $\mathbf{T}_{RN}$ are employed for translational and rotational degrees of freedom, respectively.

The complete information about the material state is to be memorised for $NG \times NLY$ points.

2.2.2. Model 2

In the present paper model 2 is confined to flat, rectangular elements only and hence the description of geometry, kinematics and stress field is simplified. In the two-dimensional middle surface the eight-node base is used with position vectors and generalised displacement vectors attached to it. The

Box 3. Flow of computations on level E for model 2 – *RSE-V*

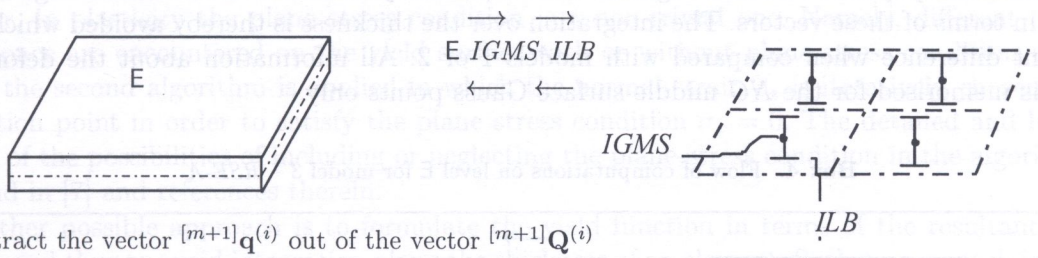

Extract the vector $^{[m+1]}\mathbf{q}^{(i)}$ out of the vector $^{[m+1]}\mathbf{Q}^{(i)}$

Loop over the Gauss points on midsurface $\zeta = 0$, $IGMS = 1, \ldots, NG$

calculate co-ordinates ξ, η

compute current generalised strain vector $^{[m+1]}\mathbf{e}^{(i)}$ and its increment $^{[m+1]}\Delta\mathbf{e}^{(i)}$ on the basis of matrix $\mathbf{B}(\xi, \eta, 0)$ and vector $\mathbf{q}$

Loop over the Lobatto points $ILB = 1, \ldots, NLB$

calculate co-ordinate ζ

compute increment of strain vector $^{[m+1]}\Delta\boldsymbol{\varepsilon}^{(i)}$

integrate incremental physical relations

Box 5 → OUTPUT: $^{[m+1]}\boldsymbol{\sigma}^{(i)}$, $^{[m+1]}\mathbf{E}^{(i)}$

add contribution of the Lobatto point ILB connected to the Gauss point $IGMS$ to:

local modular cross-section stiffness matrix $^{[m+1]}\mathbf{D}^{(i)}$

current total generalised stress vector $^{[m+1]}\mathbf{S}^{(i)}$

End of loop over ILB

Add contribution of the Gauss point $IGMS$ to:

OUTPUT a) tangent stiffness matrix $^{[m+1]}\mathbf{k}^{(i)}_{T(e)}$

OUTPUT b) current internal force vector $^{[m+1]}\mathbf{f}^{(i)}_{(e)}$

End of loop over $IGMS$

process of volume integration is different for the *RSE-V* model (Fig. 4-2) than for the *CBSE-V* one. A set of Lobatto integration points is used here instead of the pile of layers in order to discretize along the thickness direction. The Lobatto points are spread along the normal at each Gauss point of the midsurface.

Starting from the nodal displacements the generalised strains (membrane, bending and transverse shear) on the middle surface are calculated. They, in turn, are used for the calculation of strains at every Lobatto point according to the geometrical hypothesis. Here, the 'straight-director' hypothesis is applied which means the normal to an initial middle surface remains straight but not necessarily normal to the deformed surface. In the next step the physical relations are integrated at each Lobatto point with the five-element stress and strain vectors (note the variants in treating the plane stress state condition discussed below). This results in updated stress vectors as well as consistent modular matrix at each point. Finally, the integration is performed over all Lobatto points to give the resultant stresses and constitutive resultant matrix at the midsurface Gauss points. Hence, all volume integrals are transformed into surface integrals (over the midsurface as reference surface area) with all z-dependence embodied in the calculation of stress-resultant vector and constitutive resultant matrix. So, pre-integration over the thickness is followed by integration over the middle surface. Complete information about material state is to be memorised for $NG \times NLB$ points.

2.2.3. Model 3

The element to which we refer as *RSE-A* (based on area approach) is constructed in two-dimensional middle surface (Fig. 4-3). The generalised strains coupled with the stress-resultant vectors are used. The incremental physical relations together with a plasticity condition are formulated globally i.e. directly in terms of these vectors. The integration over the thickness is thereby avoided which makes significant difference when compared with models 1 or 2. All information about the deformation process is memorised for the *NG* middle surface Gauss points only.

Box 4. Flow of computations on level E for model 3 – *RSE-A*

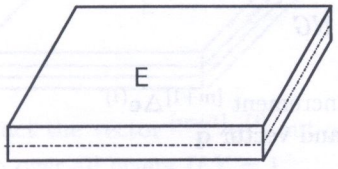

$\longrightarrow$ E *IGMS* $\longleftarrow$

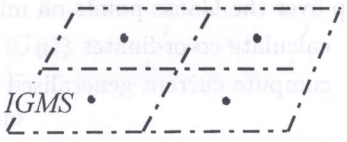

Extract the vector $^{[m+1]}\mathbf{q}^{(i)}$ out of the vector $^{[m+1]}\mathbf{Q}^{(i)}$

Loop over the Gauss points on midsurface $\zeta = 0$, $IGMS = 1, \ldots, NG$

calculate co-ordinates ξ, η

compute current generalised strain vector $^{[m+1]}\mathbf{e}^{(i)}$ and its increment $^{[m+1]}\Delta\mathbf{e}^{(i)}$ on the basis of matrix $\mathbf{B}(\xi, \eta, 0)$ and vector $\mathbf{q}$

integrate incremental physical relations

Box 6 $\rightarrow$ OUTPUT: $^{[m+1]}\mathbf{S}^{(i)}$, $^{[m+1]}\mathbf{D}^{(i)}$

Add contribution of the Gauss point *IGMS* to:

OUTPUT a)	tangent stiffness matrix	$^{[m+1]}\mathbf{k}^{(i)}_{T(e)}$
OUTPUT b)	current internal force vector	$^{[m+1]}\mathbf{f}^{(i)}_{(e)}$

End of loop over *IGMS*

2.3. Algorithms for integration of the elastic-plastic constitutive relations

The integration of the elastic-plastic constitutive relations is performed at each discretization point for every global iteration step (Box 1). Stresses, strains and process parameters on point level P are updated only after the convergence on level B is achieved. Such a treatment results in the iteration-independent integration, which for plasticity is crucial and enables us to avoid spurious plastic deformations. The presented approach is the implicit one, hence all the relations are satisfied at the end of the incremental step.

The procedure starts with a given increment of the generalised displacement vector $\Delta\mathbf{Q}$ on level B. After the transition is done to the element level E and then to point level P the strain operator results in determining the strain increments at the discretization points. Then, the incremental constitutive equations are integrated for given strain increments to result in the stresses (or generalised stresses) at these points. The integration consists of two steps. First, an elastic predictor is calculated with the linear material behaviour assumed. Then, if a plastically active process occurs i.e. the yield surface in the stress space is exceeded, a return mapping is performed to the updated yield surface. The Huber–von Mises plasticity condition is applied. For volume formulations the linear strain hardening is adopted. Material is assumed to be homogeneous and isotropic.

In the paper several approaches to the problem are applied. The first approach is called *local formulation* or *volume approach*. This means that the constitutive equations are solved at all discretization points along the thickness and then stresses are integrated to result in the generalised stresses on the middle surface. The layer model or the Lobatto quadrature is employed for along-thickness integration. In such a case the yield function is expressed in terms of stresses and (possibly) a hardening parameter. In the frame of this formulation still two different algorithms are possible. The first algorithm is based on the assumption of degenerated plane stress and plane strain state. This means the normal stress and normal strain in thickness direction are simply neglected. However, in plasticity the plane stress condition is a non-trivial one. Namely, different points in stress space are encountered on the yield surface with or without plane stress condition enforced. Hence, the second algorithm is applied in which the normal strain ε_z is iteratively chosen at each integration point in order to satisfy the plane stress condition $\sigma_z = 0$. The detailed and lucid discussion of the possibilities of including or neglecting the plane-stress condition in the algorithm can be found in [7] and references therein.

Another possible approach is to formulate the yield function in terms of the resultant stresses directly and thus to avoid integration along the thickness of an element. Such an approach is referred to as *global formulation* or *area approach* and is based on an approximation of the yield surface in terms of stress resultants [12, 20, 21]. Again, two different formulations are possible. The first is the original one (Ivanov's approach) with the assumption of full yielding throughout the thickness, which means that an element is regarded as either purely elastic (until limit capacity is reached) or purely plastic — no elastic-plastic stages are possible. The second formulation, introduced in order to moderate the above effect, is due to Crisfield [8] and enables the approximate examination of the yield zone throughout the thickness. To this end a hardening-like parameter (namely, an equivalent plastic curvature) is employed.

Details of flow charts for the computation are given in Boxes 5–8 and VI–VII. In what follows vector $\boldsymbol{\sigma}$ is either the stress vector or the stress resultant vector, depending on the formulation applied. Similarly, $\boldsymbol{\varepsilon}$ stands for either the strain vector or the generalised strain vector whereas p denotes either the hardening or the hardening-like parameter.

For all the cases the basic scheme of solution is similar [24, 19]. The elastic predictor for the stresses is calculated as

$$\boldsymbol{\sigma}^{el(i)} = \boldsymbol{\sigma}^{*} = {}^{[m]}\boldsymbol{\sigma} + \mathbf{E} \cdot (\boldsymbol{\varepsilon}^{(i)} - {}^{[m]}\boldsymbol{\varepsilon}). \tag{7}$$

Then the yield condition is checked whether

$$\Phi^{*(i)}(\boldsymbol{\sigma}^{el(i)}, {}^{[m]}p) < 0. \tag{8}$$

Box 5. Integration of the elastic-plastic relations at *GPLY* or *LBPT* points

INPUT: strain increment vector $^{[m+1]}\Delta\boldsymbol{\varepsilon}^{(i)}(\xi,\eta,\zeta)$
stress vector from last converged step $^{[m]}\boldsymbol{\sigma}(\xi,\eta,\zeta)$
hardening parameter $^{[m]}\epsilon_p(\xi,\eta,\zeta)$

Iteration loop $k = 1, 2, \ldots$

compute: first approximation $\Delta\varepsilon_z^{(0)} = \dfrac{-\nu}{1-\nu}\left(\Delta\varepsilon_x^{(i)} + \Delta\varepsilon_y^{(i)}\right)$

expanded strain increment vector $\Delta\boldsymbol{\varepsilon} = {}^{[m+1]}\Delta\boldsymbol{\varepsilon}^{(i)} + \{0\,0\,0\,0\,0\,|\Delta\varepsilon_z^{(k)}\}$

elastic predictor $\boldsymbol{\sigma}^* = {}^{[m]}\boldsymbol{\sigma} + \mathbf{E}\cdot\Delta\boldsymbol{\varepsilon}$

Check plasticity condition $\frac{1}{2}\boldsymbol{\sigma}^{*T}\mathbf{P}\,\boldsymbol{\sigma}^* - \frac{1}{3}\sigma_{pl}^2({}^{[m]}\epsilon_p) < 0$

1	**0**

elastic (passive) increment — plastic (active) increment

Calculate $\boldsymbol{\sigma}^{(i)}$, $\epsilon_p^{(i)}$, $\Delta\lambda^{(i)}$ solving the set of equations

plastic relaxation $\boldsymbol{\sigma}^{(i)} = (\mathbf{I} + \Delta\lambda^{(i)}\mathbf{EP})^{-1}\boldsymbol{\sigma}^*$

hardening param. $\epsilon_p^{(i)} = \Delta\lambda^{(i)}\sqrt{\dfrac{2}{3}\boldsymbol{\sigma}^{(i)T}\mathbf{P}\boldsymbol{\sigma}^{(i)}} + {}^{[m]}\epsilon_p$

yield condition $\dfrac{1}{2}\boldsymbol{\sigma}^{(i)T}\mathbf{P}\boldsymbol{\sigma}^{(i)} - \dfrac{1}{3}\sigma_{pl}^2(\epsilon_p^{(i)}) = 0$

Box 7: OUTPUT $\Delta\lambda^{(i)}$

$\boldsymbol{\sigma}^{(i)} = \boldsymbol{\sigma}^*$
$\mathbf{E}^{ep(i)} = \mathbf{E}$

check plane stress condition $\sigma_z^{(i)} = 0$

1	**0**

calculate:

$$A^* = \frac{\frac{4}{9}\sigma_{pl}^2(\epsilon_p^{(i)})\left.\frac{\mathrm{d}\sigma_{pl}}{\mathrm{d}\epsilon_p}\right|_{\epsilon_p^{(i)}}}{1 - \frac{2}{3}\left.\frac{\mathrm{d}\sigma_{pl}}{\mathrm{d}\epsilon_p}\right|_{\epsilon_p^{(i)}}\Delta\lambda^{(i)}}$$

$$\mathbf{E}^* = \left(\mathbf{I} + \Delta\lambda^{(i)}\mathbf{EP}\right)^{-1}\mathbf{E}$$

$$\mathbf{E}^{ep(i)} = \frac{\mathbf{E}^* - \mathbf{E}^*\mathbf{P}\boldsymbol{\sigma}^{(i)}\boldsymbol{\sigma}^{(i)T}\mathbf{P}\mathbf{E}^*}{A^* + \boldsymbol{\sigma}^{(i)T}\mathbf{P}\mathbf{E}^*\mathbf{P}\boldsymbol{\sigma}^{(i)}}$$

calculate:

if $k \geq 2$

$$\Delta\varepsilon_z^{(k+1)} = \Delta\varepsilon_z^{(k)} - \frac{\sigma_z^{(i)(k)}\left(\Delta\varepsilon_z^{(k-1)} - \Delta\varepsilon_z^{(k)}\right)}{\sigma_z^{(i)(k-1)} - \sigma_z^{(i)(k)}}$$

or

$\Delta\varepsilon_z^{(1)} = -(\Delta\varepsilon_x^{(i)} + \Delta\varepsilon_y^{(i)})$

go to next iteration, $(k) \to (k+1)$

OUTPUT: stress vector $^{[m+1]}\boldsymbol{\sigma}^{(i)}(\xi,\eta,\zeta)$
consistent tangent matrix $^{[m+1]}\mathbf{E}^{ep(i)}(\xi,\eta,\zeta)$

Box 6. Integration of the elastic-plastic relations at *GPMS* points

INPUT: generalised strain increment vector $^{[m+1]}\Delta\mathbf{e}^{(i)}(\xi,\eta)$
resultant stress vector from last converged step $^{[m]}\mathbf{S}(\xi,\eta)$
equivalent plastic curvature (hardening-like parameter) $^{[m]}\kappa_p(\xi,\eta)$

Calculate dimensionless quantities $\bar{\mathbf{S}}$, $\bar{\mathbf{e}}$

Compute: elastic predictor $\bar{\mathbf{S}}^* = {}^{[m]}\bar{\mathbf{S}} + \bar{\mathbf{E}}\,\Delta\bar{\mathbf{e}}$
dimensionless quadrature stress intensities $p_n\,,\ p_m\,,\ p_{mn}\,,\ p_t$
Crisfield's parameter $\alpha = \alpha({}^{[m]}\kappa_p)$

check plasticity condition $\Phi(p_n\,,\ p_m\,,\ p_{mn}\,,\ p_t\,,\ \alpha) < 0$	
1	**0**
↓	↓
elastic (passive) increment	plastic (active) increment

↓

Calculate $\bar{\mathbf{S}}^{(i)}, \Delta\lambda^{(i)}, \kappa_p^{(i)}$ solving the set of equations:

plastic relaxation $\bar{\mathbf{S}}^{(i)} - \left(\bar{\mathbf{S}}^{*(i)} - \bar{\mathbf{E}}\,\Delta\lambda^{(i)}\dfrac{\partial\Phi^{(i)}}{\partial\bar{\mathbf{S}}}\right)^{-1} = 0$

evolution law of Crisfield's param. $\alpha^{(i)} - f_{Cris}(\bar{S}^{(i)}, \Delta\lambda^{(i)}) = 0$

yield (plasticity) condition $\Phi^{(i)}(\bar{\mathbf{S}}^{(i)}, \alpha^{(i)}) = 0$

$\bar{\mathbf{S}}^{(i)} = \bar{\mathbf{S}}^*$
$\bar{\mathbf{D}}^{ep(i)} = \bar{\mathbf{E}}$

Box 8: OUTPUT $\bar{S}^{(i)}, \Delta\lambda^{(i)}, \alpha^{(i)}$

Calculate:

$$\mathbf{G}^{(i)T} = \left[\left(1 - \frac{\partial f_{Cris}^{(i)}}{\partial\alpha}\right)\frac{\partial\Phi^{(i)}}{\partial\bar{\mathbf{S}}}^T + \frac{\partial\Phi^{(i)}}{\partial\alpha}\,\frac{\partial f_{Cris}^{(i)}}{\partial\bar{\mathbf{S}}}^T\right]\left(\bar{\mathbf{E}}^{-1} + \Delta\lambda^{(i)}\,\frac{\partial^2\Phi^{(i)}}{\partial\bar{\mathbf{S}}^2}\right)^{-1}$$

$$\bar{\mathbf{D}}^{ep(i)} = \left(\bar{\mathbf{E}}^{-1} + \Delta\lambda^{(i)}\,\frac{\partial^2\Phi^{(i)}}{\partial\bar{\mathbf{S}}^2}\right)^{-1}\left(\mathbf{I} - \frac{\frac{\partial\Phi^{(i)}}{\partial\bar{\mathbf{S}}}\,\mathbf{G}^{(i)T}}{\mathbf{G}^{(i)T}\,\frac{\partial\Phi^{(i)}}{\partial\bar{\mathbf{S}}} - \frac{\partial\Phi^{(i)}}{\partial\alpha}\,\frac{\partial f_{Cris}^{(i)}}{\partial(\Delta\lambda)}}\right)$$

↓

return to dimensional quantities

↓

OUTPUT: resultant stress vector $^{[m+1]}\mathbf{S}^{(i)}(\xi,\eta)$
consistent tangent-resultant matrix $^{[m+1]}\mathbf{D}^{ep(i)}(\xi,\eta)$

Box 7. The Newton method algorithm for computation of $\Delta\lambda^{(i)}$

Notation: $\Delta\lambda_k^{(i)} \equiv \Delta\lambda_k\,, \quad k = 0, 1, 2, \ldots$ (superscript $^{(i)}$ omitted in expressions below)

First approximation $\Delta\lambda_0 = 0$

Iteration loop: $k = 1, 2, \ldots$

$$\Delta\lambda_{k+1} = \Delta\lambda_k - \frac{\Phi(\Delta\lambda_k)}{\left.\frac{\mathrm{d}\Phi}{\mathrm{d}(\Delta\lambda)}\right|_{\Delta\lambda_k}}$$

until $|\Phi(\Delta\lambda_k)| <$ tolerance

with

$$\Phi(\Delta\lambda) = \frac{1}{2}\boldsymbol{\sigma}^{*T}(I + \Delta\lambda\mathbf{EP})^{-1\,T} \cdot \mathbf{P} \cdot (\mathbf{I} + \Delta\lambda\mathbf{EP})^{-1}\boldsymbol{\sigma}^* - \frac{1}{3}\sigma_{pl}^2\left({}^{[m]}\epsilon_p + \Delta\lambda\sqrt{\frac{2}{3}\boldsymbol{\sigma}^{*T}(\mathbf{I} + \Delta\lambda\mathbf{EP})^{-1\,T} \cdot \mathbf{P} \cdot (\mathbf{I} + \Delta\lambda\mathbf{EP})^{-1}\boldsymbol{\sigma}^*}\right)$$

$$\frac{\mathrm{d}\Phi}{\mathrm{d}(\Delta\lambda)} = \left[1 - \left(\frac{2}{3}\right)^{\frac{3}{2}}\sigma_{pl}\frac{\mathrm{d}\sigma_{pl}}{\mathrm{d}\epsilon_p}\frac{\Delta\lambda}{\sqrt{\boldsymbol{\sigma}^T\mathbf{P}\boldsymbol{\sigma}}}\right]\frac{\mathrm{d}}{\mathrm{d}(\Delta\lambda)}\left(\frac{1}{2}\boldsymbol{\sigma}^T\mathbf{P}\boldsymbol{\sigma}\right) - \left(\frac{2}{3}\right)^{\frac{3}{2}}\sigma_{pl}\frac{\mathrm{d}\sigma_{pl}}{\mathrm{d}\epsilon_p}\sqrt{\boldsymbol{\sigma}^T\mathbf{P}\boldsymbol{\sigma}}$$

$$\frac{\mathrm{d}}{\mathrm{d}(\Delta\lambda)}\left(\frac{1}{2}\boldsymbol{\sigma}^T\mathbf{P}\boldsymbol{\sigma}\right) = \boldsymbol{\sigma}^T\mathbf{P}\frac{\mathrm{d}(\mathbf{K})}{\mathrm{d}(\Delta\lambda)}\boldsymbol{\sigma}^*$$

$$\mathbf{K} = (\mathbf{I} + \Delta\lambda\mathbf{EP})^{-1}$$

Box 8. The Newton method algorithm for solving the set of non-linear equations $\mathbf{F}(\mathbf{X}) = \mathbf{0}$

Notation: $\mathbf{X}^{(i)} = \{\bar{\mathbf{S}}^{(i)}, \Delta\lambda^{(i)}, \alpha^{(i)}\}$

$\mathbf{X}_k^{(i)} \equiv \mathbf{X}_k$ (superscript $^{(i)}$ omitted in expressions below)

First approximation $\bar{\mathbf{S}}_0 = \bar{\mathbf{S}}^*, \quad \Delta\lambda_0 = 0, \quad \alpha_0 = {}^{[m]}\alpha$

Iteration loop: $k = 1, 2, \ldots$

$$\mathbf{X}_{k+1} = \mathbf{X}_k - \left(\frac{\mathrm{d}\mathbf{F}_k}{\mathrm{d}\mathbf{X}}\right)^{-1} \cdot \mathbf{F}_k$$

until $\|\mathbf{F}(\mathbf{X}_{k+1})\| <$ tolerance

with linearization (Jacobian) matrix

$$\frac{\mathrm{d}\mathbf{F}_k}{\mathrm{d}\mathbf{X}} = \left.\begin{pmatrix} \mathbf{I} + \Delta\lambda_k\mathbf{E}\dfrac{\partial^2\Phi_k}{\partial\bar{\mathbf{S}}^2} & \mathbf{E}\dfrac{\partial\Phi_k}{\partial\bar{\mathbf{S}}} & \Delta\lambda_k\mathbf{E}\dfrac{\partial^2\Phi_k}{\partial\bar{\mathbf{S}}\,\partial\alpha} \\ \left[\dfrac{\partial\Phi_k}{\partial\mathbf{S}}\right]^T & 0 & \dfrac{\partial\Phi_k}{\partial\alpha} \\ -\left[\dfrac{\partial f_{Cris}}{\partial\bar{\mathbf{S}}}\right]^T & -\dfrac{\partial f_{Cris}}{\partial(\Delta\lambda)} & 1 - \dfrac{\partial f_{Cris}}{\partial\alpha} \end{pmatrix}\right|_{\mathbf{X}=\mathbf{X}_k}$$

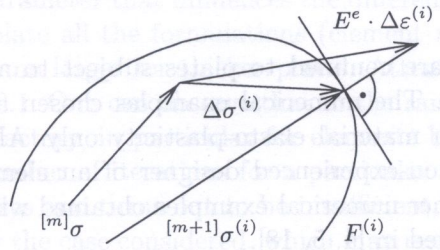

Fig. 6. Elastic predictor and return mapping

If it is not satisfied the plastic relaxation relations are built for the associative plasticity and the backward Euler scheme to give a return mapping algorithm (Fig. 6)

$$\boldsymbol{\sigma}^{(i)} = \boldsymbol{\sigma}^{el(i)} - \mathbf{E}\,\Delta\lambda^{(i)}\,\frac{\partial\Phi^{(i)}}{\partial\boldsymbol{\sigma}}\,, \tag{9}$$

where

$$\Delta\lambda^{(i)}\,\frac{\partial\Phi^{(i)}}{\partial\boldsymbol{\sigma}} = \Delta\boldsymbol{\varepsilon}^{pl(i)} \tag{10}$$

is the increment of plastic strains, and finally one comes to the set of non-linear equations in the form

$$\begin{aligned} &\boldsymbol{\sigma}^{(i)} - \boldsymbol{\sigma}^{el(i)} + \mathbf{E}\,\Delta\lambda^{(i)}\,\frac{\partial\Phi^{(i)}}{\partial\boldsymbol{\sigma}} = \mathbf{0}\,,\\ &\Phi^{*(i)}(\boldsymbol{\sigma}^{(i)}, p^{(i)}) = 0\,,\\ &f(p^{(i)}, \boldsymbol{\sigma}^{(i)}, \Delta\lambda^{(i)}) = 0\,, \end{aligned} \tag{11}$$

where the last equation is an evolution law for the hardening or hardening-like parameter p. The unknowns are the stresses (or generalised stresses, depending on formulation), plastic multiplier $\Delta\lambda$ and (if any) parameter p.

If the local formulation is chosen the above set is reduced to one non-linear equation with $\Delta\lambda^{(i)}$ as unknown (Box 7). For the global formulation the entire set is solved simultaneously (Box 8). The particular forms of vectors $\boldsymbol{\sigma}$, functions Φ or f are different for the cases discussed.

What remains is to calculate the tangent stiffness matrix for non-equilibrated configuration. To this end the plastic relaxation relations are consistently linearized with respect to $\boldsymbol{\sigma}^{(i)}$ and $\Delta\lambda^{(i)}$. Additionally, the plasticity condition is linearized and the consistency is required

$$\mathrm{d}\Phi^{(i)} = 0. \tag{12}$$

Then, after some algebra, one comes to the so-called consistent tangent matrix [23, 19] that gives the relation between increments of stresses and strains for non-equilibrated states

$$\mathrm{d}\boldsymbol{\sigma}^{(i)} = \mathbf{E}^{ep}\,\mathrm{d}\boldsymbol{\varepsilon}^{(i)}. \tag{13}$$

After the set (11) is solved and for the local formulation the stresses are integrated along the thickness to give the resultant stresses on the middle surface, the latter ones are used for the calculation of internal forces vector and residuals in global equilibrium equation. The matrix $\mathbf{E}^{ep}$ is used for updating the stiffness matrix of the global structure for the next iteration step. For the local approaches $\mathbf{E}^{ep}$ is integrated along the thickness to give such a relation for the generalised quantities on the middle surface. If the global approach is applied the latter integration is avoided.

3. NUMERICAL EXAMPLES

In the present paper examples are confined to plates subject to a transverse load with possible coupling with a membrane load. The numerical examples chosen are rather simple. Their aim is to illustrate some problems with material elasto-plasticity only. Also, the special-purpose studial code *MANKA* directed to the non-experienced designer of an element introduces restrictions for the size of a problem. Several other numerical examples obtained with the use of *MANKA* [28] and *ANKA* [16, 28] codes are published in [4, 5, 18].

The first example (Fig. 7a) is related to the results published in [19]. A plate is discretised with 3×3 serendipity plate elements. The equilibrium paths (Fig. 8) are built in the displacement–load space (Λ–w_C) with the displacement control applied ($\tau = w_C$, w_C denotes central point deflection). The efficiency of the algorithm based on the consistent linearization of the incremental physical relations and the Newton–Raphson iteration applied on level B is confirmed. It enables us to use relatively large time-like steps in the plastic range with an acceptable accuracy and a small number of global iterations. The figure collects equilibrium paths obtained for various formulations. Symbol '$*$' denotes the results from [19]. The small differences observed, in particular in the range of initial yielding, are due to the differences in discretizations on levels B, E, P, applied here and in [19]. Two groups of paths relate to either *volume* or *area* approach. The latter group, based on the Ivanov or Crisfield formulation, indicates an overestimation of the plate load carrying capacity. The Crisfield modification reduces the error with respect to the elastic limit. Here and below '*p.s.s.*' is the abbreviation for *'plane stress state'*.

Another numerical example deals with a plate in bending (Fig. 7b), made of elastic-perfectly plastic material, discretised by various models of finite elements. The slenderness of a plate (de-

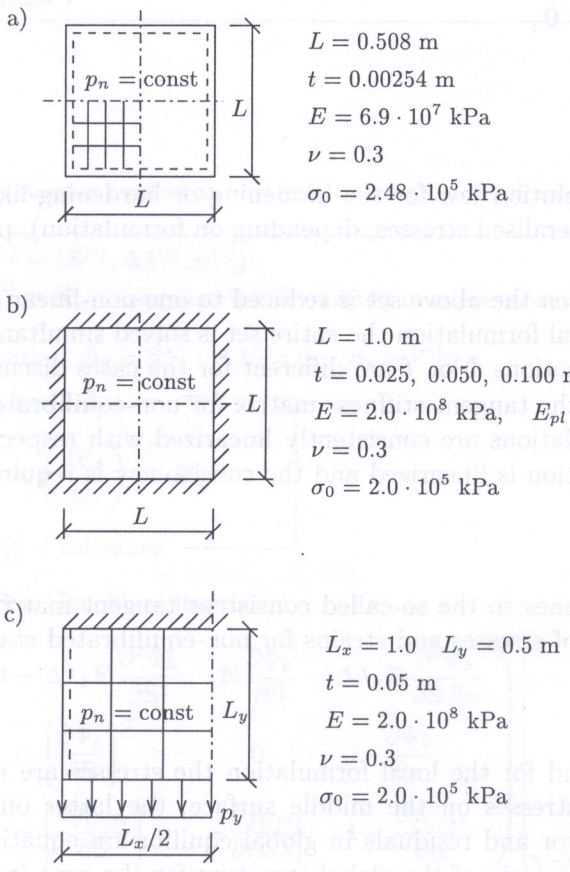

Fig. 7. Examples: loads, boundary conditions, material constants, discretizations

scribed by the ratio t/L) is a parameter that influences the differences between various formulations (Fig. 9). For the case of thin plate all the formulations (element models) lead to almost the same results. The discrepancies become larger for thicker plates. Attention is drawn to the equilibrium curves obtained for the $t/L = 0.1$. One can observe that in the range of developed plastic deformations the accuracy is not satisfactory, in particular for elements based on the *area* approach. The reason is that the allowable number of iterations for a particular incremental step is kept fixed in the code for comparison purposes and turns out to be insufficient for some cases. Also the element mesh seems to be too coarse for the case considered, which may result in artificial limit points which involve 'snap-through' effects, cf. [9].

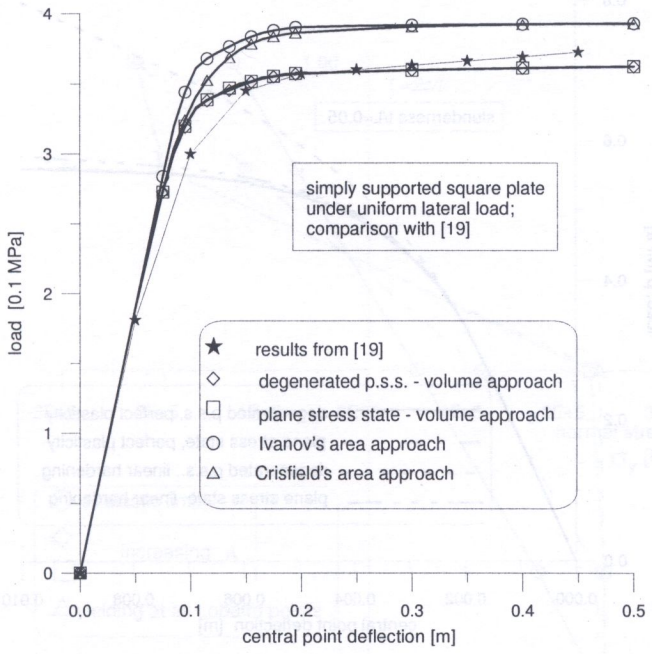

Fig. 8. Volume vs. area approach — equilibrium paths

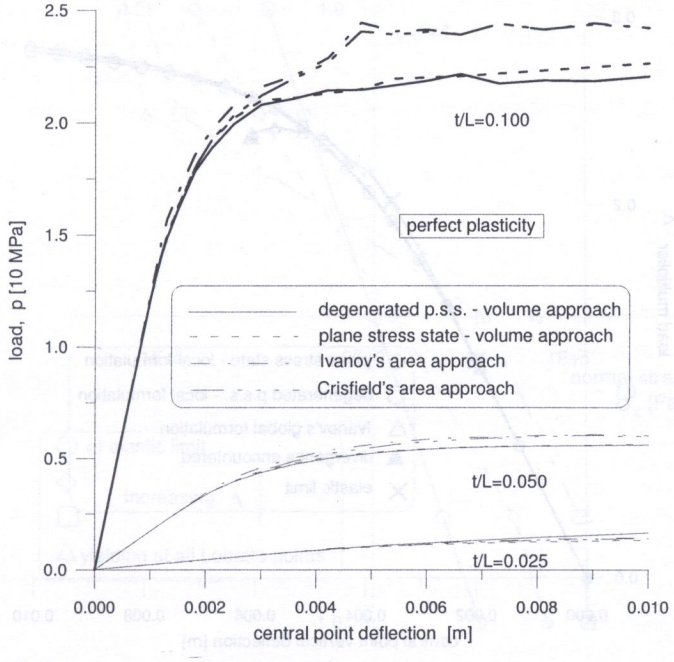

Fig. 9. Load–displacement curves for various element models and various values of plate slenderness

Figure 10 collects the equilibrium paths (load–deflection curves) for a plate of moderate thickness ($t/L = 0.05/1.0$). Perfect plasticity models are compared with linear hardening ones. Two formulations are considered: the one based on the degenerated plane stress assumption (normal stress in thickness direction is neglected) and the other based on the true plane stress condition $\sigma_z = 0$ satisfied in a way of iterative choice of the normal strain ε_z. One should note that the degenerated plane stress assumption leads to significant overestimation of plate capacity if hardening is present. This is due to inexact value of the hardening parameter ϵ_p when no normal strain in the thickness direction is included into the analysis.

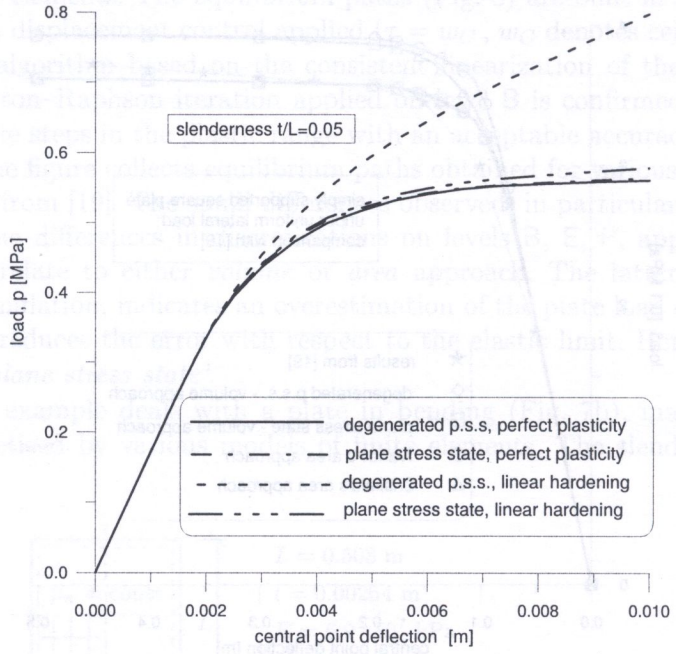

Fig. 10. Volume approach, various plane-stress conditions

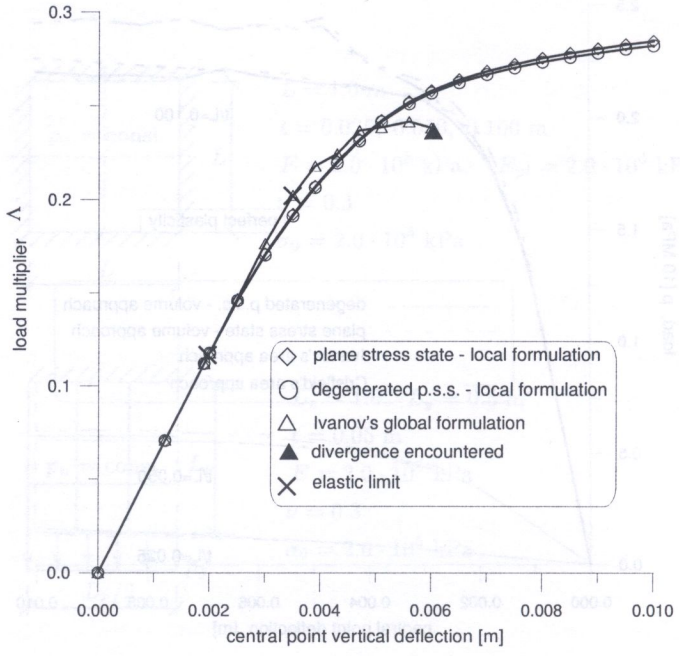

Fig. 11. Equilibrium paths for plate in bending and membrane extension

The last example deals with the superposition of bending and membrane extension of a plate (Fig. 7c). This means, in general, that on point level P all components of the stress vector or resultant stress vector are non-zero. Figure 11 presents the equilibrium curves in the load–deflection co-ordinates. The true transverse load and in-plane tension load are determined as a product of load parameter Λ and the reference load: $p_n = \Lambda \cdot 10^4\,\mathrm{kPa}$, $p_y = \Lambda \cdot 2 \cdot 10^4\,\mathrm{kN/m}$. The curve obtained with the global approach is cut because of the divergence encountered on a point level iteration. Also, one can observe an overestimation of the elastic limit capacity when compared with local approaches and a non-smooth load–deflection relation. The latter is due to too coarse discretization which induces accuracy problems for global approaches although it is good enough for the local approaches.

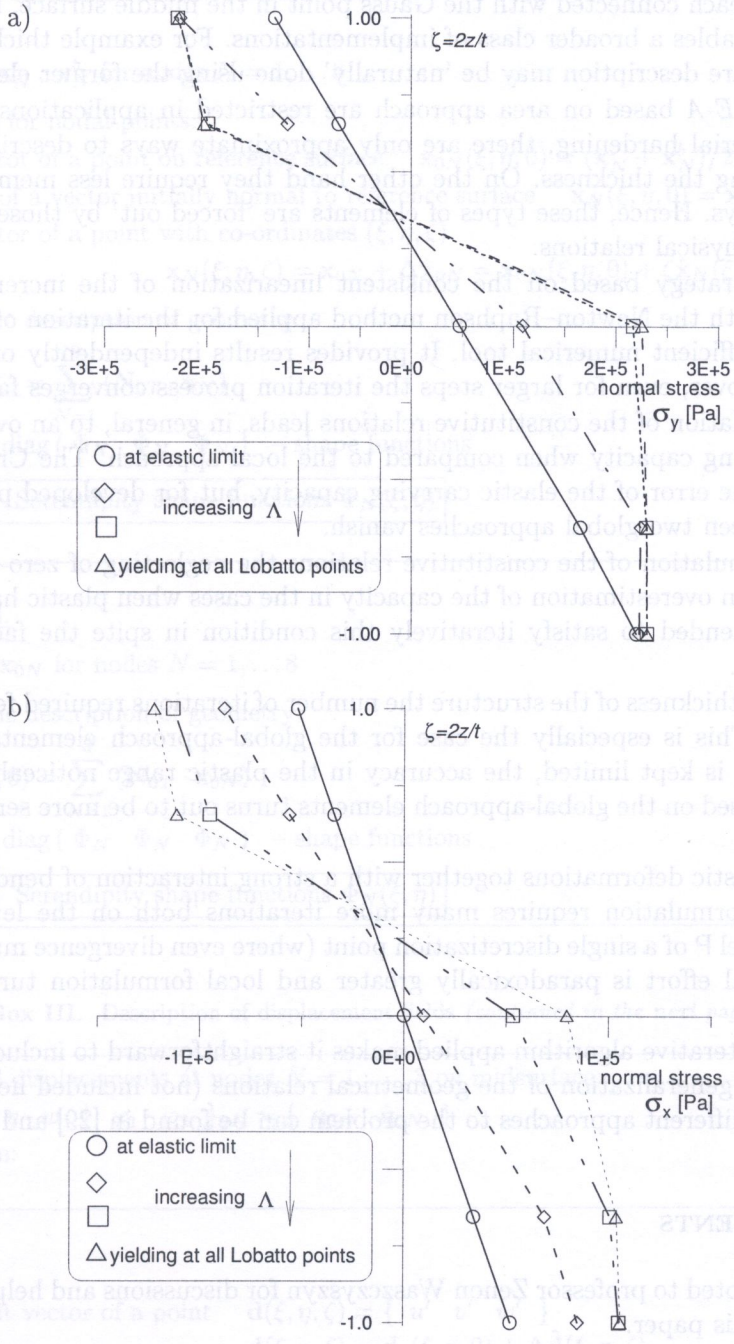

Fig. 12. Along-thickness normal stress redistribution; a) σ_y (y tension direction), b) σ_x

The along-thickness redistribution of normal stresses σ_y and σ_x for increasing values of the load parameter is presented in Figs. 12a and 12b, respectively. The stresses are taken at the most stressed point of the middle surface (closest to the clamped edge and to the symmetry axis), where first yielding occurs. Note the displacement of the neutral surface of the plate, which is due to the tension in the y direction imposed on the transverse bending.

4. Conclusions and remarks

The elements *CBSE-V* and *RSE-V* differ from each other in the manner of numerical integration. The set of layers, each discretised with the Gauss points, for the *CBSE-V* is replaced with sets of the Lobatto points, each connected with the Gauss point in the middle surface, for the *RSE-V*. The element *CBSE-V* enables a broader class of implementations. For example thick structure analysis or composite structure description may be 'naturally' done using the former element.

The elements *RSE-A* based on area approach are restricted in applications: there is no direct way to include material hardening, there are only approximate ways to describe the evolution of the plastic zone along the thickness. On the other hand they require less memory, which is not a crucial issue nowadays. Hence, these types of elements are 'forced out' by those based on the local formulation of the physical relations.

The numerical strategy based on the consistent linearization of the incremental constitutive relations together with the Newton–Raphson method applied for the iteration of global equilibrium is proved to be an efficient numerical tool. It provides results independently on the length of the time-like step. Moreover, even for larger steps the iteration process converges fast.

The global formulation of the constitutive relations leads, in general, to an overestimation of the structure load carrying capacity when compared to the local approach. The Crisfield modification allows to decrease the error of the elastic carrying capacity, but for developed plastic deformations the differences between two global approaches vanish.

For the local formulation of the constitutive relations the neglecting of zero-normal- stress condition also leads to an overestimation of the capacity in the cases when plastic hardening is present. Hence, it is recommended to satisfy iteratively this condition in spite the fact it requires more computational effort.

For an increasing thickness of the structure the number of iterations required for a given-accuracy-solution increases. This is especially the case for the global-approach elements. If the maximum number of iterations is kept limited, the accuracy in the plastic range noticeably decreases. Also, the discretization based on the global-approach elements turns out to be more sensitive to the coarse mesh effects.

For developed plastic deformations together with a strong interaction of bending and membrane loading the global formulation requires many more iterations both on the level B of the entire structure and the level P of a single discretization point (where even divergence may be encountered). Hence, the numerical effort is paradoxically greater and local formulation turns out to be more efficient.

The incremental-iterative algorithm applied makes it straightforward to include geometrical non-linearities through a generalization of the geometrical relations (not included here). The discussion and comparisons of different approaches to the problem can be found in [29] and papers cited there.

Acknowledgements

The authors are indebted to professor Zenon Waszczyszyn for discussions and helpful remarks during the preparation of this paper.

The Grant No PB 3 P404 060 06 of the Polish Committee of Scientific Research (KBN) is gratefully acknowledged for the support.

APPENDIX

Box I. Serendipity shape functions

$$\Phi_K = (1+\xi\xi_K)(1+\eta\eta_K)(\xi\xi_K+\eta\eta_K-1)/4 \qquad \text{for } K=1,3,5,7$$
$$\Phi_M = \left[\xi_M^2(1+\xi\xi_M)(1-\eta^2)+\eta_M^2(1+\eta\eta_M)(1-\xi^2)\right]/2 \qquad \text{for } M=2,4,6,8$$

Box II. Description of geometry

Model No. 1.

Input data: $\mathbf{x}_N^t$, $\mathbf{x}_N^b$ for nodes $N=1,\dots 8$

Calculations for nodal points:

Position vector of a point on reference surface $\quad \mathbf{x}_{0N}(\xi,\eta,0) = (\mathbf{x}_N^t + \mathbf{x}_N^b)/2$

Orientation of a vector initially normal to reference surface $\quad \hat{\mathbf{x}}_N(\xi,\eta,0) = \mathbf{x}_N^t - \mathbf{x}_N^b$

Position vector of a point with co-ordinates (ξ,η,ζ)

$$\mathbf{x}_N(\xi,\eta,\zeta) = \mathbf{x}_{0N} + \Delta\hat{\mathbf{x}}_{0N} = \mathbf{x}_{0N}(\xi,\eta,0) + \zeta\hat{\mathbf{x}}_N(\xi,\eta,0)/2$$

Isoparametric description of geometry:

$$\mathbf{x}(\xi,\eta,\zeta) = \sum_{N=1}^{8} (\mathbf{N}_{0T}\cdot\mathbf{x}_N)$$

$N_{0T} = \mathrm{diag}\,(\,\Phi_N \quad \Phi_N \quad \Phi_N\,)$ – shape functions

Box I: Serendipity shape functions $\Phi_N(\xi,\eta)$

Model No. 2. or 3.

Input data: $\mathbf{x}_{0N}$ for nodes $N=1,\dots 8$

Isoparametric description of geometry:

$$\mathbf{x}_0(\xi,\eta,0) = \sum_{N=1}^{8} (\mathbf{N}_{0T}\cdot\mathbf{x}_{0N})$$

$N_{0T} = \mathrm{diag}\,(\,\Phi_N \quad \Phi_N \quad \Phi_N\,)$ – shape functions

Box I: Serendipity shape functions $\Phi_N(\xi,\eta)$

Box III. Description of displacement fields *(continued in the next page)*

Nodal generalised displacements at nodes $N=1,\dots,8$ on midsurface:

$\mathbf{q}_{0N} = \{\ u \quad v \quad w \ \mid\ \varphi_1 \quad \varphi_2\ \}_{0N} = \{\ \mathbf{q}_{0N} \quad \hat{\mathbf{q}}_{0N}\ \}$

FE approximation:

Model No. 1.:

Displacement vector of a point $\quad \mathbf{d}(\xi,\eta,\zeta) = \{\ u' \quad v' \quad w'\ \}$

$$\mathbf{d}(\xi,\eta,\zeta) = \mathbf{d}_0(\xi,\eta,0) + \Delta\hat{\mathbf{d}}(\xi,\eta,\zeta)$$

FE approximation of displacements $\quad \mathbf{d}_0(\xi,\eta,0) = \mathbf{T}_T^T\left[\sum_{N=1}^{8}(\mathbf{N}_{0T}\cdot\mathbf{q}_{0N})\right]$

Box III. *(continued)* Description of displacement fields

Along-thickness displacement increment $\Delta\hat{\mathbf{d}}(\xi,\eta,\zeta) = \sum_{N=1}^{8} \left\{ \Phi_N \left[\hat{\mathbf{V}} (\mathbf{T}_{RN}^T \cdot \hat{\mathbf{q}}_{0N}) \right] \right\}$

Transformation from local to global c.s. $\mathbf{T}_T = [\ x' \quad y' \quad z'\ ]$

Transformation from local to global c.s. at a node $\mathbf{T}_{RN} = \begin{bmatrix} x'\,\mathbf{v}_{1N} & x'\,\mathbf{v}_{2N} \\ y'\,\mathbf{v}_{1N} & y'\,\mathbf{v}_{2N} \end{bmatrix}$

$\mathbf{N}_{0T} = \mathrm{diag}(\ \Phi_N \quad \Phi_N \quad \Phi_N\ )$ – shape functions

$\hat{\mathbf{V}} = (\zeta\,\mathbf{t}_N/2)\ [\ -\mathbf{v}_{2N} \quad \mathbf{v}_{1N}\ ]$

$[\ \mathbf{v}_{1N} \quad \mathbf{v}_{2N}\ ]$ – base vectors at a node

$[\ x' \quad y' \quad z'\ ]$ – base vectors at a point

Box I: Serendipity shape functions $\Phi_N(\xi,\eta)$

Model No. 2. or 3.:

Displacement of a midsurface point $\mathbf{d}(\xi,\eta,0) = \{\ u \quad v \quad w \quad \theta_1 \quad \theta_2\ \}$

FE approximation of displacements $\mathbf{d}_0(\xi,\eta,0) = \sum_{N=1}^{8} (\mathbf{N}_{0TR} \cdot \mathbf{q}_{0N})$

Shape functions $\mathbf{N}_{0TR} = \mathrm{diag}(\ \Phi_N \quad \Phi_N \quad \Phi_N \mid \Phi_N \quad \Phi_N)$

Box I: Serendipity shape functions $\Phi_N(\xi,\eta)$

Box IV. Description of strain and stress fields, kinematic and physical relations *(continued in the next page)*

Model No. 1.

For every $ILY = 1,\ldots,NLY$ — at every $GPLY$ point with co-ordinates $(\xi,\eta,\zeta)_{IGLY}$

Definition of strain vector: $\boldsymbol{\varepsilon} = \{\ \varepsilon_{x'} \quad \varepsilon_{y'} \quad \gamma_{x'y'} \quad \gamma_{x'z'} \quad \gamma_{y'z'}\ \}$

Strain–displacement relation:

$$\{\ \varepsilon_{x'} \quad \varepsilon_{y'} \quad \gamma_{x'y'} \quad \gamma_{x'z'} \quad \gamma_{y'z'}\ \} = \{\ u'_{,x'} \quad v'_{,y'} \quad u'_{,y'}+v'_{,x'} \quad u'_{,z'}+w'_{,x'} \quad v'_{,z'}+w'_{,y'}\ \}$$

$${}^{[m+1]}\boldsymbol{\varepsilon}^{(i)} = \mathbf{B}(\xi,\eta,\zeta) \cdot {}^{[m+1]}\mathbf{q}^{(i)}$$

Strain increment vector: ${}^{[m+1]}\Delta\boldsymbol{\varepsilon}^{(i)} = {}^{[m+1]}\boldsymbol{\varepsilon}^{(i)} - {}^{[m]}\boldsymbol{\varepsilon}^{(last)}$

Definition of stress vector: $\boldsymbol{\sigma} = \{\ \sigma_x \quad \sigma_y \quad \tau_{xy} \quad \tau_{xz} \quad \tau_{yz}\ \}$

Stress–strain incremental relations: ${}^{[m+1]}\Delta\boldsymbol{\sigma}^{(i)} = {}^{[m+1]}\mathbf{E}^{(i)} \,.\, {}^{[m+1]}\Delta\boldsymbol{\varepsilon}^{(i)}$

Stress vector ${}^{[m+1]}\boldsymbol{\sigma}^{(i)} = {}^{[m]}\boldsymbol{\sigma}^{(last)} + {}^{[m+1]}\Delta\boldsymbol{\sigma}^{(i)}$

Constitutive matrix: ${}^{[m+1]}\mathbf{E}^{(i)}(\xi,\eta,\zeta)$

For every $GPMS$ with co-ordinates $(\xi,\eta,0)$

Resultant stress vector: ${}^{[m+1]}\mathbf{S}^{(i)} = \sum_{ILY} \left\{ {}^{[m+1]}\boldsymbol{\sigma}^{(i)}(\xi,\eta,\zeta) \cdot \Delta\zeta_{ILY} \cdot t/2 \right\}$

Box IV. *(continued)* Description of strain and stress fields, kinematic and physical relations

Model No. 2.

For midsurface at every *GPMS* point with co-ordinates $(\xi, \eta, 0)$

Definition of generalised strain vector: $\mathbf{e} = \{ e_x \;\; e_y \;\; \gamma_{xy} \;\; \kappa_x \;\; \kappa_y \;\; \chi_{xy} \;\; \gamma_{xz} \;\; \gamma_{yz} \}$

Strain–displacement relation:

$$\{ e_x \;\; e_y \;\; \gamma_{xy} \;\; \kappa_x \;\; \kappa_y \;\; \chi_{xy} \;\; \gamma_{xz} \;\; \gamma_{yz} \}$$
$$= \{ u_{,x} \;\; v_{,y} \;\; u_{,y}+v_{,x} \;\; \theta_{2,x} \;\; -\theta_{1,y} \;\; \theta_{2,y}-\theta_{1,x} \;\; \theta_2+w_{,x} \;\; -\theta_1+w_{,y} \}$$

$$^{[m+1]}\mathbf{e}^{(i)} = \mathbf{B}_0(\xi, \eta, 0) \cdot {}^{[m+1]}\mathbf{q}^{(i)}$$

Strain increment vector $^{[m+1]}\Delta\mathbf{e}^{(i)} = {}^{[m+1]}\mathbf{e}^{(i)} - {}^{[m]}\mathbf{e}^{(last)}$

For every *LBPT* point with co-ordinates $(\xi, \eta, \zeta)_{IGMS}$ for $\zeta = 2z/t$

Definition of strain vector: $\boldsymbol{\varepsilon} = \{ \varepsilon_x \;\; \varepsilon_y \;\; \gamma_{xy} \;\; \gamma_{xz} \;\; \gamma_{yz} \}$

Strain increment vector: $\Delta\boldsymbol{\varepsilon}(\xi, \eta, \zeta) = \mathbf{H}(\zeta \cdot t/2) \cdot \Delta\mathbf{e}(\xi, \eta, 0)$

'Hypothesis' matrix $\mathbf{H}(z) = \begin{bmatrix} 1 & 0 & 0 & z & 0 & 0 & 0 & 0 \\ 0 & 1 & 0 & 0 & z & 0 & 0 & 0 \\ 0 & 0 & 1 & 0 & 0 & z & 0 & 0 \\ 0 & 0 & 0 & 0 & 0 & 0 & 1 & 0 \\ 0 & 0 & 0 & 0 & 0 & 0 & 0 & 1 \end{bmatrix}$

Definition of stress vector: $\boldsymbol{\sigma} = \{ \sigma_x \;\; \sigma_y \;\; \tau_{xy} \;\; \tau_{xz} \;\; \tau_{yz} \}$

Stress–strain incremental relations: $^{[m+1]}\Delta\boldsymbol{\sigma}^{(i)} = {}^{[m+1]}\mathbf{E}^{(i)} \,.\, {}^{[m+1]}\Delta\boldsymbol{\varepsilon}^{(i)}$

Stress vector: $^{[m+1]}\boldsymbol{\sigma}^{(i)} = {}^{[m]}\boldsymbol{\sigma}^{(last)} + {}^{[m+1]}\Delta\boldsymbol{\sigma}^{(i)}$

Pre-integration through the thickness

Constitutive-resultant matrix: $^{[m+1]}\mathbf{D}^{(i)}(\xi, \eta, 0) = \int_t (\mathbf{H}^T\mathbf{E}\mathbf{H})\,\mathrm{d}z$

Resultant stress: $^{[m+1]}\mathbf{S}^{(i)}(\xi, \eta, 0) = \int_t (\mathbf{H}^T\boldsymbol{\sigma})\,\mathrm{d}z$

Model No. 3.

For midsurface at every *GPMS* point with co-ordinates $(\xi, \eta, 0)_{IGMS}$

Definition of generalised strain vector $\mathbf{e} = \{ e_x \;\; e_y \;\; \gamma_{xy} \;\; \kappa_x \;\; \kappa_y \;\; \chi_{xy} \;\; \gamma_{xz} \;\; \gamma_{yz} \}$

Strain–displacement relation:

$$\{ e_x \;\; e_y \;\; \gamma_{xy} \;\; \kappa_x \;\; \kappa_y \;\; \chi_{xy} \;\; \gamma_{xz} \;\; \gamma_{yz} \}$$
$$= \{ u_{,x} \;\; v_{,y} \;\; u_{,y}+v_{,x} \;\; \theta_{2,x} \;\; -\theta_{1,y} \;\; \theta_{2,y}-\theta_{1,x} \;\; \theta_2+w_{,x} \;\; -\theta_1+w_{,y} \}$$

$$^{[m+1]}\mathbf{e}^{(i)} = \mathbf{B}_0(\xi, \eta, 0)^{[m+1]}\mathbf{q}^{(i)}$$

Strain increment vector $^{[m+1]}\Delta\mathbf{e}^{(i)} = {}^{[m+1]}\mathbf{e}^{(i)} - {}^{[m]}\mathbf{e}^{(last)}$

Definition of stress resultant vector $\mathbf{S} = \{ n_x \;\; n_y \;\; n_{xy} \;\; m_x \;\; m_y \;\; m_{xy} \;\; t_x \;\; t_y \}$

Stress–strain incremental relations: $^{[m+1]}\Delta\mathbf{S}^{(i)} = {}^{[m+1]}\mathbf{D}^{(i)} \,.\, {}^{[m+1]}\Delta\mathbf{e}^{(i)}$

Constitutive-resultant matrix: $^{[m+1]}\mathbf{D}^{(i)}$

Box V. Matrices **k** and vectors **f** of elements *(continued in the next page)*

Model No. 1.

Stiffness matrix

$$\mathbf{k}_T = \iiint_V (\mathbf{B}^T\mathbf{E}\mathbf{B})\,\mathrm{d}V \approx \sum_{ILY} \Delta t_{ILY} \left\{ \iint_\Omega (\mathbf{B}^T\mathbf{E}\mathbf{B})\,\mathrm{d}\Omega_{ILY} \right\}$$

$$= \sum_{ILY} \left\{ \Delta t_{ILY} \sum_{IGLY} [(\mathbf{B}^T\mathbf{D}\mathbf{B}) \cdot \det \mathbf{J} \cdot W] \right\}_{IGLY}$$

Internal force vector

$$\mathbf{f} = \iiint_V (\mathbf{B}^T\boldsymbol{\sigma})\,\mathrm{d}V \approx \sum_{ILY} \Delta t_{ILY} \left\{ \iint_\Omega (\mathbf{B}^T\boldsymbol{\sigma})\,\mathrm{d}\Omega_{ILY} \right\}$$

$$= \sum_{ILY} \left\{ \Delta t_{ILY} \sum_{IGLY} [(\mathbf{B}^T\boldsymbol{\sigma}) \cdot \det \mathbf{J} \cdot W] \right\}_{IGLY}$$

W_{IGLY} – Gauss quadrature weights

Model No. 2.

$$\mathbf{S} = \int_t \mathbf{H}^T(z) \cdot \boldsymbol{\sigma}(z)\,\mathrm{d}z \approx \frac{t}{2} \sum_{ILB} [(\mathbf{H}^T(z) \cdot \boldsymbol{\sigma}(z)) \cdot W]_{ILB}$$

$$\mathbf{D} = \int_t \mathbf{H}^T(z)\,\mathbf{E}(z)\,\mathbf{H}(z)\,\mathrm{d}z \approx \frac{t}{2} \sum_{ILB} [(\mathbf{H}^T(z)\,\mathbf{E}(z)\,\mathbf{H}(z)) \cdot W]_{ILB}$$

with $z = \frac{t}{2}\zeta_{ILB}$, ζ_{ILB} – Lobatto quadrature nodes, W_{ILB} – Lobatto quadrature weights

Stiffness matrix $\mathbf{k}_T = \iint_{\Omega_0} (\mathbf{B}^T\mathbf{D}\mathbf{B})\,\mathrm{d}\Omega_0 \approx \sum_{IGMS} [(\mathbf{B}^T\mathbf{D}\mathbf{B}) \cdot \det \mathbf{J}_0 \cdot W]_{IGMS}$

Internal force vector $\mathbf{f} = \iint_{\Omega_0} (\mathbf{B}^T\mathbf{S})\,\mathrm{d}\Omega_0 \approx \sum_{IGMS} [(\mathbf{B}^T\mathbf{S}) \cdot \det \mathbf{J}_0 \cdot W]_{IGMS}$

W_{IGMS} – Gauss quadrature weights

Model No. 3.

Stiffness matrix $\mathbf{k}_T = \iint_{\Omega_0} (\mathbf{B}^T\mathbf{D}\mathbf{B})\,\mathrm{d}\Omega_0 \approx \sum_{IGMS} [(\mathbf{B}^T\mathbf{D}\mathbf{B}) \cdot \det \mathbf{J}_0 \cdot W]_{IGMS}$

Internal force vector $\mathbf{f} = \iint_{\Omega_0} (\mathbf{B}^T\mathbf{S})\,\mathrm{d}\Omega_0 \approx \sum_{IGMS} [(\mathbf{B}^T\mathbf{S}) \cdot \det \mathbf{J}_0 \cdot W]_{IGMS}$

W_{IGMS} – Gauss quadrature weights

Box VI. Definitions and formulae (volume approach)

Elasticity matrices (E — Young's modulus, ν— Poisson's ratio):

for degenerated plane stress state (σ_z neglected) $\mathbf{E} = \dfrac{E}{1-\nu^2}\begin{pmatrix} 1 & \nu & 0 & 0 & 0 \\ \nu & 1 & 0 & 0 & 0 \\ 0 & 0 & \frac{1-\nu}{2} & 0 & 0 \\ 0 & 0 & 0 & \frac{1-\nu}{2} & 0 \\ 0 & 0 & 0 & 0 & \frac{1-\nu}{2} \end{pmatrix}$

for 3D stress state ($\nu \neq 0.5$) $\mathbf{E} = \dfrac{E}{(1+\nu)(1-2\nu)}\begin{pmatrix} 1-\nu & \nu & 0 & 0 & 0 & \nu \\ \nu & 1-\nu & 0 & 0 & 0 & \nu \\ 0 & 0 & \frac{1-2\nu}{2} & 0 & 0 & 0 \\ 0 & 0 & 0 & \frac{1-2\nu}{2} & 0 & 0 \\ 0 & 0 & 0 & 0 & \frac{1-2\nu}{2} & 0 \\ \nu & \nu & 0 & 0 & 0 & 1-\nu \end{pmatrix}$

for 3D stress state ($\nu = 0.5$) $\mathbf{E} = \dfrac{E}{1+\nu}\begin{pmatrix} 1 & 0 & 0 & 0 & 0 & 0 \\ 0 & 1 & 0 & 0 & 0 & 0 \\ 0 & 0 & \frac{1}{2} & 0 & 0 & 0 \\ 0 & 0 & 0 & \frac{1}{2} & 0 & 0 \\ 0 & 0 & 0 & 0 & \frac{1}{2} & 0 \\ 0 & 0 & 0 & 0 & 0 & 1 \end{pmatrix}$

Plasticity matrices:

for degenerated plane stress state $\mathbf{P} = \begin{pmatrix} \frac{2}{3} & -\frac{1}{3} & 0 & 0 & 0 \\ -\frac{1}{3} & \frac{2}{3} & 0 & 0 & 0 \\ 0 & 0 & 2 & 0 & 0 \\ 0 & 0 & 0 & 2 & 0 \\ 0 & 0 & 0 & 0 & 2 \end{pmatrix}$

for three dimensional stress state $\mathbf{P} = \begin{pmatrix} \frac{2}{3} & -\frac{1}{3} & 0 & 0 & 0 & -\frac{1}{3} \\ -\frac{1}{3} & \frac{2}{3} & 0 & 0 & 0 & -\frac{1}{3} \\ 0 & 0 & 2 & 0 & 0 & 0 \\ 0 & 0 & 0 & 2 & 0 & 0 \\ 0 & 0 & 0 & 0 & 2 & 0 \\ -\frac{1}{3} & -\frac{1}{3} & 0 & 0 & 0 & \frac{2}{3} \end{pmatrix}$

Material hardening description (in uniaxial tension with σ_0 – yield point stress):

perfect plasticity: $\sigma_{pl} = \sigma_0\,, \quad \dfrac{\mathrm{d}\sigma_{pl}}{\mathrm{d}\epsilon_p} = 0$

linear hardening (with E_{pl} – hardening module): $\sigma_{pl} = \sigma_0 + E_{pl}\epsilon_p\,, \quad \dfrac{\mathrm{d}\sigma_{pl}}{\mathrm{d}\epsilon_p} = E_{pl}$

non-linear asymptotic hardening ($\sigma_{pl} \to k\sigma_0$): $\sigma_{pl} = \sigma_0 \dfrac{1+k\rho\epsilon_p}{1+\rho\epsilon_p}\,, \quad \dfrac{\mathrm{d}\sigma_{pl}}{\mathrm{d}\epsilon_p} = \dfrac{\rho}{(1+\rho\epsilon_p)^2}$

(with k, ρ — parameters)

Box VII. Definitions and formulae (area approach)

Dimensional: resultant stress vector, generalised strain vector and elasticity matrix

$$\mathbf{S} = \mathbf{V}_S \cdot \bar{\mathbf{S}} = \{\, n_x \;\; n_y \;\; n_{xy} \;\; m_x \;\; m_y \;\; m_{xy} \;\; t_x \;\; t_y \,\}$$

$$\mathbf{e} = \mathbf{V}_e \cdot \bar{\mathbf{e}} = \{\, \epsilon_x \;\; \epsilon_y \;\; \gamma_{xy} \;\; \kappa_x \;\; \kappa_y \;\; \chi_{xy} \;\; \gamma_{xz} \;\; \gamma_{yz} \,\}$$

$$\mathbf{E} = \mathbf{V}_S^{-1}\, \bar{\mathbf{E}}\, \mathbf{V}_e = \frac{Et}{1-\nu^2} \begin{pmatrix} 1 & & & & & & & \\ \nu & 1 & & & & & & \\ 0 & 0 & \frac{1-\nu}{2} & & & \text{sym} & & \\ 0 & 0 & 0 & \frac{t^2}{12} & & & & \\ 0 & 0 & 0 & \frac{\nu t^2}{12} & \frac{t^2}{12} & & & \\ 0 & 0 & 0 & 0 & 0 & \frac{t^2(1-\nu)}{24} & & \\ 0 & 0 & 0 & 0 & 0 & 0 & \frac{1-\nu}{2} & \\ 0 & 0 & 0 & 0 & 0 & 0 & 0 & \frac{1-\nu}{2} \end{pmatrix}$$

with dimension diagonal matrices

$$\mathbf{V}_e = \operatorname{diag}\left(1,\, 1,\, 1,\, \frac{1}{t},\, \frac{1}{t},\, \frac{1}{t},\, 1,\, 1\right) \qquad \mathbf{V}_S = \sigma_0\, t \cdot \operatorname{diag}\left(1,\, 1,\, 1,\, \frac{t}{4},\, \frac{t}{4},\, \frac{t}{4},\, 1,\, 1\right)$$

t – thickness, E – Young's modulus, ν – Poisson's ratio, σ_0 – uniaxial yield point stress

Dimensionless quadrature generalised stress intensities

$$P_n = \bar{n}_x^2 + \bar{n}_y^2 - \bar{n}_x\, \bar{n}_y + 3\bar{n}_{xy}^2$$

$$P_m = \bar{m}_x^2 + \bar{m}_y^2 - \bar{m}_x\, \bar{m}_y + 3\bar{m}_{xy}^2$$

$$P_{nn} = \bar{n}_x\, \bar{m}_x + \bar{n}_y\, \bar{m}_y - 0.5(\bar{n}_y\, \bar{m}_x + \bar{n}_x\, \bar{m}_y) + 3\bar{n}_{xy}\, \bar{m}_{xy}$$

$$P_t = 3\bar{t}_x^2 + 3\bar{t}_y^2$$

Yield function

$$\Phi = P_n + P_t + 0.5\left(\frac{P_m}{\alpha^2} + \frac{1}{\alpha}\sqrt{\frac{P_m^2}{\alpha^2} + 4P_{mn}^2}\right) - \frac{(P_n + P_t)P_m - P_{mn}^2}{4[\alpha^2(P_n + P_t) + 0.48P_m]} - 0.24\sqrt{\frac{P_t|P_{mn}|}{\alpha}} - 1$$

Evolution law for the Crisfield parameter

$$\alpha = f_{Cris}(\kappa_p) = 1 - 0.4\, \exp\left(-2.6\sqrt{\kappa_p + \beta}\right)$$

$$\kappa_p = {}^{[m]}\kappa_p + \frac{2E}{3\sqrt{3}\sigma_0}\, \Delta\lambda \sqrt{\left(\frac{\partial \Phi}{\partial \bar{m}_x}\right)^2 + \left(\frac{\partial \Phi}{\partial \bar{m}_y}\right)^2 + \frac{\partial \Phi}{\partial \bar{m}_x}\frac{\partial \Phi}{\partial \bar{m}_y} + \frac{1}{4}\left(\frac{\partial \Phi}{\partial \bar{m}_{xy}}\right)^2}$$

β – small parameter

REFERENCES

[1] J. Bielski. *A Semi Analytical Approach to the Analysis of Elastic-Plastic Imperfect Shells of Revolution.* Report LR-745, Delft University of Technology, 1994.

[2] J. Bielski. A global plasticity formulation combined with a semi-analytical analysis of imperfect shells of revolution. *Thin-Walled Struct.*, **23**: 399–411, 1995.

[3] J. Bielski. A note on the consistent linearization of the global approach to plasticity in thin shell analysis. Submitted to *Thin-Walled Struct.*, 1996.

[4] J. Bielski, M. Radwańska, R. Gawęda. *Nonlinear Analysis of Surface Structures, Part I, II* (in Polish). Report No. B-11/96, B-12/96, Institute of Computer Methods in Civil Engineering, Cracow University of Technology, 1996.

[5] J. Bielski, M. Radwańska. On elastic-plastic finite elements for nonlinear analysis of surface structures. *Proc. XIII Polish Conf. "Computer Methods in Mechanics", Poznań*, Vol. **1**: 157–166, 1997.

[6] M. Bischoff, E. Ramm. Three-dimensional shell formulation and elements for large deformations. In: H.A. Mang and F.G. Rammerstorfer, eds., *IUTAM Symp. On Discretization Methods in Structural Mechanics*, 27–34. Kluwer Academic Publishers, The Netherlands, 1999.

[7] R. de Borst. The zero-normal-stress condition in plane-stress and shell elastoplasticity. *Communications in Applied Numerical Methods,* **7**: 29–33, 1991.

[8] M.A. Crisfield. *Ivanov's Yield Criterion for Thin Steel Plates and Shells Using Finite Elements.* TRRL Report LR 919, Crowthorne, England, 1979.

[9] M.A. Crisfield, X. Peng. Instabilities induced by coarse meshes for a nonlinear shell problem. *Engineering Computations*, **13**(6): 110–114, 1996.

[10] W. Gilewski, M. Radwańska. A survey of finite element models for the analysis of moderately thick shells. *FEAD*, **9**: 1–21, 1991.

[11] E. Hinton, D.R.J. Owen. *Finite Element Software for Plates and Shells.* Pineridge Press Ltd., Swansea, UK, 1984.

[12] G.V. Ivanov. Approximation of the finite relationship between forces and moments in shell subject to the Mises yield condition (in Russian). *Inzh. Zhurnal Mekh. Tverdogo Tela*, **6**: 74–75, 1967.

[13] C. Miehe. A theoretical and computational model for isotropic elastoplastic stress analysis in shells at large strains. *Comp. Meth. Appl. Mech. Engng.*, **155**: 193–233, 1998.

[14] C. Miehe, S. Schley. Large-strain thermoplastic analysis of shell-like structures. In: O.T. Bruhns, ed., *Grosse plastiche Formanderungen, Bad Honnef 1997*, 127–136, *Mitteilungen aus dem Institute fur Mechanik, Ruhr-Universitat, Bochum,* **114**, 1998.

[15] E. Pabisek, Z. Waszczyszyn. Consistent algorithm of solving of the incremental elastic-plastic equations on a point and structure level (in Polish). *Proc. IX Polish Conf. "Computer Methods in Mechanics", Kraków-Rytro*, 851–858, 1989.

[16] E. Pabisek. *ANKA v.2 — User's Manual* (in Polish). Report No. B-14/96, Institute of Computer Methods in Civil Engineering, Cracow University of Technology, 1996.

[17] M. Radwańska. Degenerated shell elements in the context of shell theories of first and second approximation. *Proc. 5th Conf. Shell Structures, Theory and Applications, Warsaw-Janowice*, 31–41, 1992.

[18] M. Radwańska, J. Pamin, E. Pabisek, R. Gawęda. Inelastic finite elements in ANKA computer code. *Proc. XIII Polish Conf. "Computer Methods in Mechanics", Poznań*, Vol. **3**, 1115–1122, 1997.

[19] E. Ramm, A. Matzenmiller. Computational aspect of elasto-plasticity in shell analysis. In: D.R.J. Owen, ed., *Proc. Computational Plasticity, Barcelona.* Pineridge Press, 711–734, 1987.

[20] M. Robinson. A comparison of yield surfaces for thin shells. *Int. J. Mech. Sci.*, **13**: 345, 1971.

[21] M. Robinson. The effect of transverse shear stresses on the yield surface for thin shells. *Int. J. Solids Structures*, **9**: 819–828, 1973.

[22] J.C. Simo, J.G. Kennedy. On a stress resultant geometrically exact shell model. Part V. Nonlinear plasticity: formulation and integration algorithms. *Comp. Meth. Appl. Mech. Engng.*, **96**: 133–171, 1992.

[23] J.C. Simo, R.L. Taylor. Consistent tangent operators for rate-independent elastoplasticity. *Comp. Meth. Appl. Mech. Engng*, **48**: 101–118, 1985.

[24] J.C. Simo, R.L. Taylor. A return mapping algorithm for plane stress analysis. *Int. J. Num. Meth. Eng.*, **22**: 649–670, 1986.

[25] G.M. Stanley, K.C. Park, T.J. Hughes. Continuum-based resultant shell elements. In: T.J.R. Hughes et al., eds., *Finite Element Methods for Plates and Shell Structures*, Vol. **1**: *Element Technology.* Pineridge Press, Swansea, 1–45, 1986.

[26] Z. Waszczyszyn. *Computational Methods in Plasticity.* Report LR-583, Delft University of Technology, 1989.

[27] Z. Waszczyszyn. Some basic problems of the finite element analysis of elastoplastic structures (a survey). *Mech. Teor. Stos.*, **28**(1-2): 255–275, 1990.

[28] Z. Waszczyszyn, C. Cichoń, M. Radwańska. *Stability of Structures by Finite Element Methods.* Elsevier, Amsterdam, 1994.

[29] P. Wriggers, R. Eberlein, S. Reese. A comparison of three-dimensional continuum and shell elements for finite plasticity. *Int. J. Sol. Struct.*, **33**: 3309–3326, 1996.

[30] M. Ziyaeifar, A.E. Elwi. Degenerated plate-shell elements with refined transverse shear strains. *Computers and Structures*, **60**(6): 1079–1091, 1996.

[31] M. Życzkowski. *Combined Loadings in the Theory of Plasticity.* PWN (Polish Scientific Publishers), Warsaw, 1981.